THE VIRTUAL SOURCE METHOD FOR IMAGING STEEPLY DIPPING STRUCTURES USING A WALK-AWAY VSP ACQUISITION GEOMETRY

EMMA BRAND

THE VIRTUAL SOURCE METHOD FOR IMAGING STEEPLY DIPPING STRUCTURES USING A WALK-AWAY VSP ACQUISITION GEOMETRY

by

© Emma Brand

A thesis submitted to the

School of Graduate Studies

in partial fulfillment of the

requirements for the degree of

Master of Science

Department of Earth Sciences

Memorial University of Newfoundland

October 2010

St. John's Newfoundland

Abstract

Seismic interferometry is a recently developed geophysical technique that has been used almost exclusively to solve imaging problems in petroleum environments. It is a method that has a broad range of applications, however one of the most well-known is the ability of the technique to create virtual sources at the location of buried receivers, without knowledge of the subsurface velocity between the true surface sources and the receivers. This research focuses on a problem in a minerals environment, in which a shallow, steeply dipping sub-surface feature is to be illuminated using the virtual source method, a form of seismic interferometry. The research presented here uses both a ray tracing analysis and 2D synthetic seismic modelling to understand the implementation issues associated with the virtual source method. The ultimate aim is to understand the acquisition and processing requirements to image optimally a shallow, steeply dipping sub-surface feature in a hard rock environment.

Acknowledgments

I would like to thank the following people for their support of this project:

Dr. Chuck Hurich for all his supervision and advice with regards to all aspects of this project. I would also like to thank Dr. Hurich for providing me with the opportunity to continue my studies at Memorial University.

Dr. Jeremy Hall for all his advice and support.

Dr. Sharon Deemer for all her technical advice.

Dr. Phil Bording for giving me the initial opportunity to study at Memorial University.

Alexander Keith for being there every Friday night.

Finally, I'd like to thank my mates for their friendship, and my family, who have always supported my endeavours, no matter what.

Table of Contents

List of Tables

List of Figures

List of Equations

List of Appendices

Chapter 1 Introduction

Due to source-receiver geometry, conventional surface seismic reflection surveys are very good at imaging horizontally oriented lithological layers (Figure 1a). Unfortunately many geological structures of interest are not oriented horizontally; steeply dipping mineral bearing dykes or petroleum reserves trapped on the flanks of salt domes are of interest in the mineral and petroleum industries respectively. Imaging these targets with conventional surface seismic techniques is difficult not only due to source-receiver geometry, but also due to complex overburden velocity distributions which blur the final seismic image. Vertical Seismic Profiles (VSP) have been used since the 1950's to calibrate surface seismic data, provide time to depth relationships and accurate seismic velocities (Oristaglio, 1985). VSP's typically consist of a surface seismic source and receivers located in a subsurface borehole. This acquisition geometry is useful for imaging steeply dipping features due to the more favourable source-receiver geometry (Figure 1b). However the seismic data recorded by VSP's are affected by the complex overburden through which the wavefield, generated by surface sources, must travel. This heterogeneous velocity field can defocus the seismic energy and produce a poorly resolved seismic image.

The virtual source method, a form of seismic interferometry, is a relatively new geophysical technique which has the power to create virtual sources at the location of

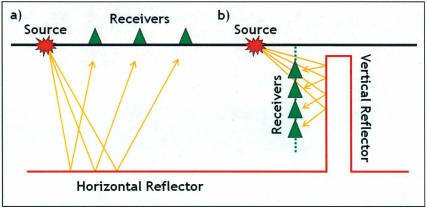

Figure 1. Illumination of Horizontal and Vertical Reflectors.

The yellow lines represent the approximate the ray path of the reflected wavefield that is recorded by the receivers.

a) The surface source-receiver geometry best illuminates horizontal reflectors; b) The VSP geometry best illuminates vertical reflectors. Note however, that any arbitrarily oriented subsurface target can be seismically imaged provided the reflected wavefield is recorded by the survey receivers. In practice, depending on the aperture of the seismic survey, this typically means that features with 90° dip (ie. are vertical) are at the extreme imaging limit for surface seismic surveys. Overhanging features (ie. with dips greater than 90°) are almost impossible to image with surface seismic surveys. VSP's typically have a more favourable source-receiver geometry for imaging overhanging features especially if the borehole is deviated to parallel the reflection surface.

buried receivers *without knowledge* of the complex overburden velocities. What makes this technique so unique is that there is no other method that can perform this redatuming without an estimate of the velocities between the original datum and the new datum. More importantly however, by redatuming the source closer to the target structure, the virtual source method has the potential to better resolve hard-to-image steeply dipping subsurface features. A review of the historical developments of the virtual source method, together with an overview of the applications of the method, is presented in Chapter 2.

For this study we investigate the virtual source method as a technique for imaging shallow, steeply dipping features, such as feeder dykes to an ore body. An example of such a geological scenario are the feeder dykes to the main ore body at Voisey's Bay mine, located in northern Labrador, Canada (Figure 2). Chapter 3 presents a simple ray tracing analysis of the virtual source method. This chapter develops the concept of the image ray and investigates capturing this image ray in practice, including the impact of VSP acquisition geometries.

Chapter 4 demonstrates how virtual source data is generated and includes an analysis of the pre-stack, CMP-sorted virtual source gathers and the final stacked and migrated virtual source image. This chapter also demonstrates the importance of understanding which image rays have been captured, as this allows for the generation of the optimal virtual source image.

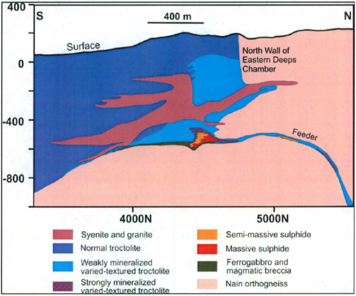

Figure 2. Cross Section of Voisey's Bay Ovoid.

The feeder dykes at the Voisey's Bay Mine are an example of the type of imaging problem being considered by this research. The deposition and geometry of the massive sulphide at Voisey's Bay is partly controlled by pre-existing sub-vertical brittle structures. Imaging of the sub-vertical structures, particularly those associated with mineralization would be a major adjunct to the drilling program associated with underground deposit evaluations and development of a mine plan. From Naldrett and Li, 2007.

Chapter 5 discusses the practical implementation of the virtual source method for several different walk-away VSP geometries and velocity and density fields. This chapter also investigates how to optimize surface source spacing in order to balance the imaging requirements of the virtual source method and the environmental and economic costs associated with data acquisition.

Finally Chapter 6 reiterates the motivation for this research and presents the conclusions drawn from the ray tracing analysis and 2D synthetic modeling.

Chapter 2 Review of the Virtual Source Method

2.1 Terminology

Seismic interferometry as a geophysical technique is currently being investigated by many researchers across the world, such that agreement on common terminology and an overarching theoretical framework is still evolving. For instance the methods of interferometric imaging, seismic interferometry, acoustic daylight imaging, time-reversed acoustics and the virtual source method all share the same general process of trace cross correlation and summation however all are derived from an independent theoretical basis (Schuster and Zhou, 2006). Thus in order to avoid confusion, this author will follow the convention (that appears to be gaining traction in the literature) that any general process utilizing cross correlation and summation will be referred to as seismic interferometry.

It should be noted however, that the research presented here grew out of questions posed in a mining geophysics context and the terminology employed is therefore consistent with that used in the mining industry and not necessarily the geophysical literature. With this in mind, the specific method discussed here will be termed the virtual source method and should not be confused with the virtual source method as pioneered by Bakulin and Calvert (2004, 2005, 2006, 2008).

To avoid confusion, the definition of key terms is made here. Locally, within the text, the meaning of additional terms will be clarified.

Seismic Interferometry: an umbrella term to describe any independently derived algorithm that uses cross correlation and summation to produce virtual sources.

Virtual Source method: the specific seismic interferometric method implemented in this study.

Virtual Source Receiver: the real downhole receiver that will be converted into a virtual source via a cross correlation and summation procedure.

Image Receiver: the real downhole receiver that is cross correlated against the virtual source receiver.

Receiver Pair: consists of the virtual source receiver and the corresponding image receiver.

Virtual Source CMP: the common mid-point of a receiver pair.

Virtual Source CMP offset: the distance between the virtual source receiver and the corresponding image receiver in a receiver pair.

Correlation trace: The trace produced via the cross correlation of a receiver pair.

Correlation gather: A common receiver-pair gather containing a collection of correlation traces. Each trace in the gather is the product of the cross correlation of a receiver pair, but for different source locations. The correlation gather is produced prior to the summation process. The summation of the correlation gather produces a single trace.

Virtual Source trace: produced by the summation of the traces in a correlation gather.

Virtual Source gather: the gather produced by the cross correlation and summation process of the virtual source method. It is a collection of virtual source traces, sorted by common virtual source, that is, each trace in the gather has the virtual source receiver, in the receiver pair, in common.

Virtual Source CMP gather: the virtual source data sorted by virtual source common mid-points.

Image Ray: the ray required to obtain the correct kinematic application of the cross correlation technique.

Image Ray Geometry: the ray path geometry required to obtain the correct kinematic application of the cross correlation technique.

Image Ray Fold: the total number of image rays which contribute to a virtual source CMP location. If all image rays are present then the image ray fold is equal to the virtual source CMP fold.

Image Ray Offsets: the CMP offsets satisfied by the captured image rays.

2.2 Historical Development of Seismic Interferometry

Seismic interferometry is an umbrella term to describe any method with the common implementation of trace cross correlation and summation. The information inherent in the autocorrelation of seismic data has been known for well over 50 years. For instance Horton (1955) used the autocorrelation process to characterize the nature of seismic noise. Claerbout (1968) however, was the first to recognize the importance of the autocorrelation function in seismic interferometry. He was able to demonstrate mathematically that "the reflection seismogram from a surface source and a surface receiver is one side of the autocorrelation of the seismogram from a source at depth and the same receiver". That is, the reflection response of the layered medium can be generated by autocorrelation of its transmission response. Claerbout's (1968) research implied that passive noise sources generated in the earth and recorded at the surface can be used to determine the earth's reflectivity response, that is create an image of the subsurface. Claerbout (1968) also demonstrated that the cross correlation of two traces recorded at locations A and B results in a trace *equivalent* to the trace that would be recorded at B due to a source at A. This process extracts the impulse response between two receivers, as if one of the receivers was a virtual source, and is referred to by those in the geophysics exploration industry as the reflection response, and by seismologists and physicists as the Green's function (Wapenaar et al., 2006). This mathematical development is based on specular ray-path assumptions in a horizontally layered half-space, and is referred to as acoustic daylight imaging (Rickett and Claerbout, 1999).

In 2000 Gerald T. Schuster, during a sabbatical stay at the Stanford Exploration Project, spent time investigating the information available in seismic trace cross correlations (Wapenaar et al., 2006). It was through this research that Schuster (2001) applied the cross correlation technique to active seismic data that is, seismic data generated with man-made sources. Schuster (2001) extended Claerbout's (1968) development to include arbitrary distributions of sources and reflectivity by validating the theory using stationary phase arguments. Simultaneously at the Delft Applied Geophysics group, Wapenaar et al. (2002) developed a general proof for arbitrary (acoustic and elastic) heterogeneous 3D media using a reciprocity theorem. Draganov et al. (2003) subsequently confirmed this proof using numerical models in heterogeneous media.

Independent of the field of geophysics, Fink (1992) published the results of physical models, measured with ultrasonic transducers, demonstrating that strongly scattered wavefields could be time-reversed and back-propagated through complex media to produce a focused wavefield. His work inspired the development of the virtual source method as presented by Bakulin and Calvert (2004, 2005, 2006, 2008), which utilizes the properties of time-reversal to generate mathematically virtual sources at the location of seismic receivers.

2.3 Applications of the Virtual Source Method

Seismic interferometry is typically implemented in two general forms:

1. Passive seismic acquisition, whereby random noise signals emitted from within the earth are recorded at the surface and the cross correlation and summation method is used to extract reflectivity information. This form of the method is typically referred to as interferometric imaging or acoustic daylight imaging.

2. Active seismic acquisition, whereby sources or receivers are buried and via the cross correlation and summation procedure, virtual sources are generated at the receiver locations without knowledge of the subsurface velocities between the sources and receivers. This form of seismic interferometry is the focus of the research presented in this thesis.

Over the past decade seismic interferometry has been used on real data for time-lapse seismic monitoring (Bakulin and Calvert, 2004; Yu et al., 2009; Zhou et al., 2008), the suppression of surface waves (Vasconcelos et al., 2008; Xue et al., 2009), statics and redatuming (Henley, 2008; Lu et al., 2007), and imaging the flanks of salt domes (Hornby and Yu, 2006; Lu et al., 2009; Willis et al., 2006; Xiao et al., 2006; Yu and Hornby, 2007). This study is focused on seismic interferometry for illuminating steeply dipping structures using a controlled source walk-away VSP geometry, similar to that described by Hornby and Yu (2006), Yu and Hornby (2007) and Schuster (2009) who refers to this type of seismic interferometry as the VSP (Vertical Seismic Profile) → SWP (Single Well Profile) correlation transform. Willis et al. (2006) use a method referred to as time-reversed acoustics to image salt-flanks also with a walk-away VSP geometry. Xiao et al. (2006) described a novel use of seismic interferometry to migrate transmitted P- to S-waves in VSP data in order to image salt-flanks. The research undertaken in this thesis however most closely resembles the method described by Hornby and Yu (2006) and Yu and Hornby (2007).

The focus of previous research has been soft-rock environments. This study is original in that it is being applied to a problem in a minerals environment. Specifically, the study is focused on the optimal acquisition and processing parameters required to produce the virtual source image of a shallow, steeply dipping subsurface target hosted in a hard rock setting. Due to the absence of significant inhomogeneity in shallow hard rock environments, a straight-ray tracing analysis is appropriate to understand how the virtual source method is formulated in theory and can be applied in practice.

Chapter 3 Ray Tracing Analysis of the Virtual Source Method

3.1 Introduction

There are several different robust mathematical derivations of the virtual source method based on representation theorems (Wapenaar, 2004) or time-reversed imaging (Bakulin and Calvert, 2006). These derivations however are difficult to understand intuitively. Ray tracing on the other hand is a simple technique that can be employed with modest effort, but provide maximum insight into the virtual source method. A straight ray analysis is particularly appropriate for a hard rock problem due to the absence of turning waves. The following is therefore a geometric analysis of the method from a ray tracing perspective, for a simple vertical reflector in a homogeneous field.

3.2 The Image Ray

Consider the simple VSP scenario: two buried receivers, separated from a vertical subsurface reflection boundary, record direct and reflected events generated by a single surface source (Figure 3a). The surface source is offset from the buried receivers and emits a zero phase wavelet (Figure 3b). This ray path geometry is conceived specifically so that *Receiver A records a direct event whose path coincides with the specular ray reflection at Receiver B*. For this geometry, Receiver A records a direct event (DA) at $\sqrt{8}$ units and a reflected event (WA) at $\sqrt{40}$ units (Figure 3c, Figure 4a), whilst Receiver B records a direct event (DB) at $\sqrt{40}$ units and a reflected event (WB) at $\sqrt{72}$ units (Figure 3c, Figure 4b).

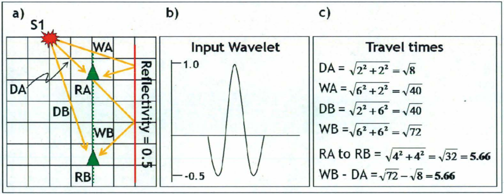

Figure 3. **Simple Ray Tracing Model.**

Where:

DA – Direct event recorded at Receiver A;

WA – Specularly reflected event recorded at Receiver A;

DB – Direct event recorded at Receiver B;

WB – Specularly reflected event recorded at Receiver B.

Direct and specularly reflected events are recorded at Receivers A and B. Note that the specular reflection at Receiver B (WB) has the same ray path as the direct event at Receiver A (DA). This is the required image ray geometry. We note that the difference in travel time between WB and DA is equal to the travel time for a specularly reflected ray from Receiver A to B.

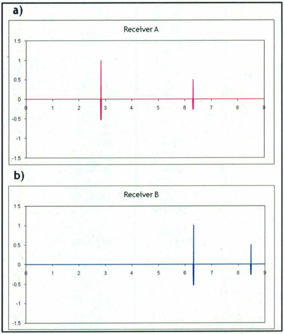

Figure 4. Receiver Records.

a) Receiver A records a direct event at $\sqrt{8}$ units and a reflected event at $\sqrt{40}$ units; b) Receiver B records a direct event at $\sqrt{40}$ units and a reflected event at $\sqrt{72}$ units.

Cross correlation of the recorded traces produces four events (Figure 5a). Each event in the correlation trace represents the time difference between the events recorded at Receiver A and the events recorded at Receiver B. Because of the specific ray path geometry chosen, the travel time *difference* between the direct event at Receiver A and the reflected event at Receiver B is equal to the *total travel time* for a reflected event emanating from Receiver A and recorded at Receiver B (Figure 6). Thus cross correlation of the direct event at A and the reflected event at B will produce a trace with one event whose travel time is equal to the specular reflection from a source at A to a receiver at B (Figure 5b).

The setup as outlined in Figure 3 is the ray path geometry required to obtain the correct kinematic application of the cross correlation technique. That is, to obtain the correct time information from the correlation trace. This ray path geometry is termed the image ray geometry (Figure 6). If the image ray geometry is not satisfied then the travel time of the event in the correlation trace will still represent the travel time difference between the direct event at Receiver A and the reflected event at Receiver B. However it will *not be equal* to the total travel time for a reflected event emanating from a source at A and recorded at B (Figure 7).

This highlights a fundamental problem with the cross correlation method; in reality there is no way of actually knowing the image ray geometry, and therefore it is impossible to obtain

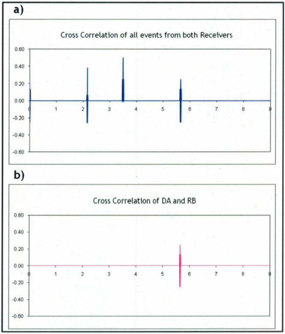

Figure 5. Cross Correlation Lags.

a) Cross correlation of all recorded events. Four events are computed. The timing of these events corresponds to the travel time difference between the events recorded at A and the events recorded at B; b) Cross correlation of the direct event at A and the reflected event at B only. Only one event is computed for which the total travel time is equal to the time difference between the direct event at A and the reflected event at B.

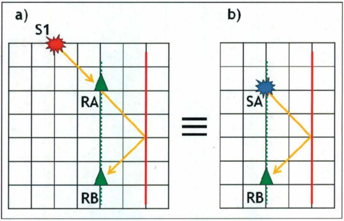

Figure 6. Image Ray Geometry.

For the specific specular ray path geometry indicated here, the travel time difference a) between the direct event at Receiver A and the reflected event at Receiver B is equivalent to the total travel time b) for an event emanating from a source at A, reflecting off the vertical boundary and being recorded at Receiver B. This is the ray path geometry required for correct kinematic application of the correlation technique.

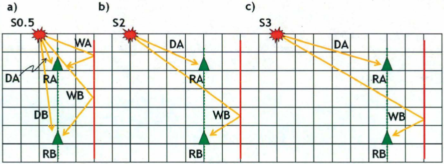

Travel Times		
S0.5	S2	S3
DA = $\sqrt{5}$ WB = $\sqrt{61}$	DA = $\sqrt{20}$ WB = $\sqrt{100}$	DA = $\sqrt{40}$ WB = $\sqrt{136}$
WB - DA = 5.57	WB - DA = 5.53	WB - DA = 5.34

Figure 7. Violation of the Image Ray Geometry.

As the source spacing changes the travel time difference between the direct arrival at Receiver A (DA) and the reflected arrival at Receiver B (WB) no longer equals the travel time for an event emanating from a source at A, reflecting off the vertical boundary and being recorded at Receiver B, which for this specific geometry is 5.66 units. Note that the position of the vertical reflecting boundary will also influence the source-receiver geometry required for correct kinematic application of the correlation technique.

the correct kinematic application of the cross correlation technique. Fortunately this problem can be overcome in both theory and in practice.

3.3 Capturing the Image Ray in Practice

Consider now the relatively more complex walk-away VSP scenario: eleven buried receivers, separated from a vertical subsurface boundary, record direct and reflected events generated by surface sources (Figure 8a). Surface sources are offset from the buried receivers and each emit a zero phase wavelet (Figure 8b). Using the geometric method utilized for the simple single source VSP model (Section 3.2), travel times for direct and reflected events emanating from each source and recorded at each receiver are computed. Refer to Appendix A for the Fortran code utilized to generate the data in Section 3.3.

For each receiver pair in the model there exists a source location that satisfies the required image ray geometry. As noted earlier however, an accurate reflector location will not be known in practice, and thus the correct image ray geometry cannot be predetermined. Fortunately due to the mathematical setup of the virtual source theory this problem can be overcome. Schuster (2001) demonstrated that the integral equations defining the virtual source method require that buried receivers be surrounded completely by a continuous distribution of surface sources. In practice, the numerical solution to this integral requires summation of the correlation traces over all sources. This summation process results in the *destructive interference of all incorrectly located events and constructive interference*

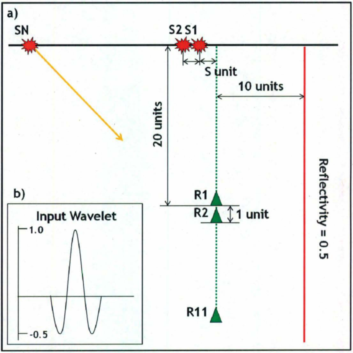

Figure 8. More Complex Ray Tracing Model.

a) The model here simulates a walk-away VSP acquisition geometry with source spacing of S units. The first source is located S units to the left of the surface location of the well. Receiver 1 is buried 20 units below the surface and 10 units horizontally from the vertical reflector, with reflectivity of 0.5. 11 receivers are located in the vertical well, all 1 unit apart. b) The input wavelet is a simple centrally peaked wavelet with half amplitude side-lobes.

of the correctly located events. This is due to the integral possessing a stationary phase point such that the solution to the integral will asymptote to a stationary value, provided the limits are sufficiently large and the integration points sufficiently dense. In this way the correct, kinematically located event is extracted from the recorded dataset without explicit subsurface velocity information or knowledge of the required image ray geometry. This is a testament to the power of the virtual source method. It should be noted that the stationary phase derivation of the virtual source method is best for simple models, where the contributions from the different sources are easy to trace. More robust derivations based on representation theorems or time-reversed imaging, are applicable to more complex geometries and heterogeneous velocity / density models (Snieder et al., 2006). The benefit of this analysis however, is that is it easier to understand the derivation of the virtual source technique and therefore the acquisition requirements of the method.

In practice however, it is unrealistic to expect a geophysical survey to be able to provide a continuous distribution of surface sources. Fortunately a discrete array of sources is sufficient to satisfy the requirements of the virtual source theory (Korneev and Bakulin, 2006). Significant care however must be taken in the selection of the acquisition geometry such that two aspects of the virtual source imaging technique are satisfied. The first is that the aperture of surface sources be broad enough to capture the required image rays (Yu and Hornby, 2007). The second is that the surface sources are dense enough to ensure effective destructive interference of the incorrectly located events, that is, the non-stationary phase contributions (Mehta et. al., 2008). These aspects are due to the practical implementation of the numerical solution to the integral equations defining the virtual source method. In this practical implementation the source aperture is analogous to the integral limits, and the source density is analogous to the integration points.

To evaluate the importance of ensuring the source aperture is wide enough to capture the required image rays, three experiments are undertaken using a simple walk-away VSP acquisition geometry (Figure 8). The experiments involve increasing the number of surface sources from 10 shots (Figure 9a, Figure 10a) to 50 shots (Figure 9b, Figure 10b), to 100 shots (Figure 9c, Figure 10c) whilst keeping the source spacing constant at 1 unit. Thus the surface source aperture is increased with each experiment. As the number of sources increases the number of correlation traces in each correlation gather increases (Figure 9). The subsequent virtual source gathers (Figure 10) better represent the true image (Figure 10d). This is because the image rays become captured by the increasingly broad surface source aperture, such that the numerical solution to the integral asymptotes to the stationary point. The practical implementation issues associated generating an optimal virtual source image given a finite source aperture will be demonstrated in Chapter 4.

To demonstrate the importance of source spacing in ensuring effective interference of the incorrectly located events, another three experiments are undertaken. Again, the simple

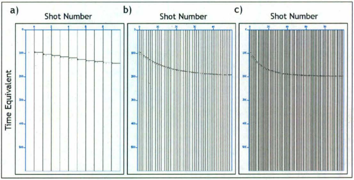

Figure 9. Correlation Gathers for a Constant Source Density.

a) 10 Shots; b) 50 Shots; c) 100 Shots. Each correlation gather contains a collection of correlation traces. Each trace is computed from the cross correlation of a specific receiver pair for a specific shot. In this case each correlation trace represents the cross correlation of Receiver 1 with Receiver 2. The summation of the traces in the correlation gather will produce a single trace, called the virtual source trace, that will represent the trace that would be recorded if a source was located at Receiver 1 and the response was recorded at Receiver 2. Whilst the model presented here violates the requirement that sources completely surround buried receivers, the importance of capturing the image ray is evident. For as the source aperture increases the integral limits increase and the numerical solution to the integral asymptotes to the stationary point.

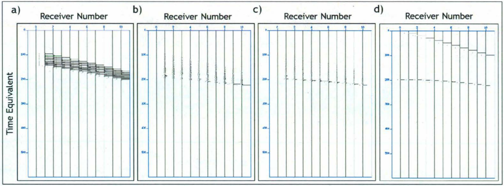

Figure 10. Virtual Source Gathers for a Constant Source Density.

a) 10 Shots; b) 50 Shots; c) 100 Shots; d) Synthetic Forward model. Each virtual source gather contains a collection of virtual source traces. Each trace is computed from the cross correlation of a specific receiver pair and summed over all shots. In this case the first virtual source trace represents the cross correlation of Receiver 1 with Receiver 2 and summed over all shots; the second virtual source trace represents the cross correlation of Receiver 1 with Receiver 3 and summed over all shots, and so on. Thus this virtual source gather represents the data that would be recorded if a source was located at Receiver 1 and recorded at all other receivers. As the source aperture increases so too does the integral limits and the numerical solution to the integral asymptotes to the stationary point in the correlation gathers, and subsequently a better virtual source gather is obtained

walk-away VSP acquisition geometry is utilized (Figure 8). For these experiments the total source aperture of 100 units is kept constant, whilst the total number of sources is increased from 25 (Figure 11a, Figure 12a) to 50 (Figure 11b, Figure 12b) to 100 (Figure 11c, Figure 12c). As the total source density is increased, the source spacing decreased and the horizontal distance between the incorrectly located events is reduced (Figure 11). Thus the stacking process results in better destructive interference of the non-stationary phase contributions (Figure 12). Mehta et al. (2008) refer to the poor destructive interference as spatial aliasing, and noted that the correlation gathers which contain a large slope in the cross correlation event will be more vulnerable to this effect. The practical implementation issues associated with surface source spacing will be discussed in Chapter 5.

These rudimentary results demonstrate that the practical implementation of the virtual source method requires a wide enough source aperture and a sufficiently dense source distribution. These parameters are analogous to the integration limits and integration points required for the numerical solution to the virtual source integral.

As a final observation for this particular acquisition geometry we note that the walk-away VSP surface source distribution fails to generate an up-going image ray. That is, there are no virtual source contributions to receivers shallower than the virtual source under consideration (Figure 13). This has been recognized by Yu and Hornby (2007) who only sum traces in the correlation gather that contribute to the stationary phase waves.

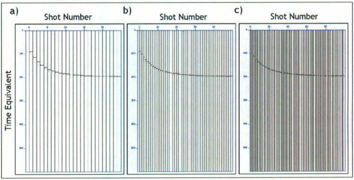

Figure 11. Correlation Gathers for Constant Source Aperture.

a) 25 Shots; b) 50 Shots; c) 100 Shots. Each correlation gather contains a collection of correlation traces. Each trace is computed from the cross correlation of a specific receiver pair for a specific shot. In this case each correlation trace represents the cross correlation of Receiver 1 with Receiver 2. The summation of the traces in the correlation gather will produce a single trace, called the virtual source trace that will represent the trace that would be recorded if a source was located at Receiver 1 and the response was recorded at Receiver 2. Whilst the model presented here violates the requirement that sources completely surround the buried receivers, the importance of source density is evident. For as the source density increases the non-stationary phase points are better sampled.

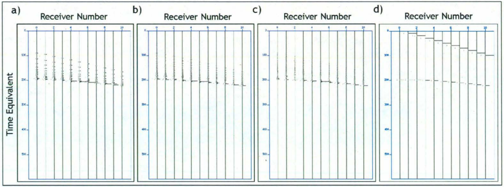

Figure 12. Virtual Source Gathers for Constant Source Aperture.

a) 25 Shots; b) 50 Shots; c) 100 Shots; d) Synthetic Forward model. Each virtual source gather contains a collection of virtual source traces. Each trace is computed from the cross correlation of a specific receiver pair and summed over all shots. In this case the first virtual source trace represents the cross correlation of Receiver 1 with Receiver 2 and summed over all shots; the second virtual source trace represents the cross correlation of Receiver 1 with Receiver 3 and summed over all shots, and so on. Thus this virtual source gather represents the data that would be recorded if a source was located at Receiver 1 and recorded at all other receivers. As the source density increases the incorrectly located events are better sampled in the correlation gathers, and subsequently a better virtual source gather is obtained.

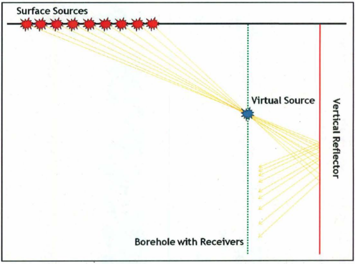

Figure 13. Implications of VSP Acquisition Geometry on Virtual Source Imaging.

For this specific imaging scenario, the vertical reflector combined with the surface walk-away VSP source distribution will never produce an up-going image ray geometry. This means that each virtual source will effectively only illuminate sections of the vertical reflector deeper than its downhole location.

3.4 Impact of VSP Geometries on the Virtual Source Data

The previous section (3.3) demonstrated that the application of seismic interferometry for generating virtual sources at the location of buried receivers is valid despite violating the requirement that buried receivers be completely surrounded by sources. This is fortunate, for in practice it is impossible to surround completely buried receivers with sources. One aspect of the technique that cannot be violated however is the requirement that the image ray be captured. If the image ray is not captured then the virtual source data generated by the cross correlation and summation process will incorrectly locate the reflection events (Figure 7). It is therefore very important that seismic surveys are designed to capture these image rays, as well as ensure that the source spacing is optimized such that the integral solution is properly sampled. Ray tracing analysis of a particular acquisition geometry enables us to determine which image rays will be captured using a certain surface source aperture. By determining the image ray geometry, we can project the rays back to the surface to compute the required location of the surface sources (Figure 14a). By understanding where the surface sources are required to satisfy all the image rays we can begin to determine the affects of using a realistic surface source aperture on the virtual source data. Additionally, by understanding which traces contribute to the virtual source image we can optimize not only the acquisition parameters, but also the processing parameters.

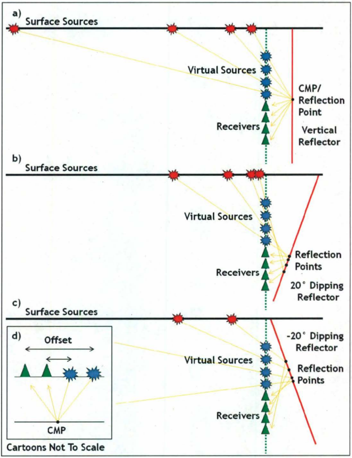

Figure 14. Virtual Source Geometry.

To address this issue for the walk-away VSP survey, a simplified hard rock model is utilized (Figure 15). The model is homogeneous, except for a vertical interface. A parallel borehole and reflector is used to simplify the ray tracing analysis. For this analysis we also consider it the worst-case imaging scenario since we ignore the situation in which the feature is dipping towards the borehole (Figure 14). This is because features dipping towards the borehole tend to be seismically invisible due to the source-receiver configuration (Figure 14c). Conversely, features dipping away from the borehole can be imaged with a smaller surface source aperture (Figure 14b). Different VSP geometries are modelled in order to understand the effects of source aperture, receiver spacing and reflector location on the virtual source geometry of the virtual source survey (Figure 15, Table 1). Refer to Appendix B for the Fortran code utilized to generate the data in Section 3.4.

3.4.1 Determining the Virtual Source Geometry

The geometry of the virtual source survey is controlled by the number of downhole receivers and their spacing. This is because the downhole receiver locations also represent the location of the virtual sources. This information allows for the calculation of virtual source survey geometries such as CMP offset, CMP location and CMP fold. Note that unless explicitly stated otherwise, all reference to CMP location and CMP fold refers to the virtual source geometry and not the VSP geometry. As per conventional seismic surveys, it is important that the geometry of the virtual source survey be sufficient to image the target reflector. An additional complication for the virtual source survey however is the

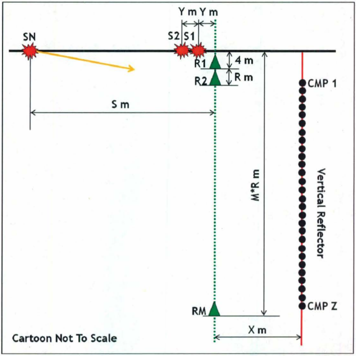

Figure 15. Minerals-Style Walk-Away VSP Model.

The model here represents a more realistic hard rock walk-away VSP acquisition geometry. The vertical borehole is situated X m away from a vertical reflector. M number of receivers starting at 4 m downhole are spaced R m apart to a total depth of M*R m. The walk-away VSP acquisition geometry consists of N shots with source aperture of S m with a source spacing of Y m. The first source is located 8 m to the left of the surface location of the well. The black dots represent the approximate CMP locations for the receiver geometry. The actual parameters used in the different models are detailed in Table 1.

Table 1. Ray Tracing Models.

Parameters tested in the ray tracing models in order to understand better the acquisition parameters for generating virtual source data. Parameters are defined in Figure 15. Values varying from Baseline Model 1 are highlighted in gray.

Model		Source Aperture (S m)	Receiver Spacing (R m)	Number of Receivers (M)	Reflector distance from Borehole (X m)	Total Number of CMP's (Z)	Depth to Bottom of Borehole (M*R m)
Number	Name						
1	Baseline 1	N/A	4	300	250	597	1204
1a	Source Spacing	1440	4	300	250	597	1204
2	Baseline 2 – Receiver Spacing	N/A	8	150	250	397	1204
2a	Source Spacing	1440	8	150	250	397	1204
3	Baseline 3 – Reflector Location	N/A	4	300	500	597	1204
3a	Source Spacing	1440	4	300	500	597	1204

requirement that the image rays also be satisfied. Using an estimate for the location of the target reflector, the required image rays can be calculated. Using straight ray analysis these image rays can then be projected to the surface and the actual surface source location can be determined (Figure 14a). If for some reason these surface source locations can't be satisfied by the actual walk-away VSP survey, this analysis allows us to determine which image rays will not be captured. The image ray fold is a measure of how many image rays contribute to a specific CMP location. The image ray offsets are the CMP offsets that are satisfied by the image rays. If all image rays are satisfied then the image ray fold for a particular CMP location is equal to the CMP fold, and the image ray offsets are equal to the CMP offsets.

This is a powerful analysis in that, provided a good estimate of the target reflector is available, noisy traces, those that contain no real virtual source information, can be excluded from the final virtual source image thereby increasing the signal to noise ratio of the data.

3.4.2 Effect of Surface Source Aperture

Source aperture and density are two very important factors when planning a seismic survey, not only in terms of imaging, but also for economic and environmental considerations. The ray tracing analysis undertaken so far has also highlighted the importance of both source aperture and density to the success of the virtual source method. It is therefore important to understand these factors in both an imaging and acquisition sense for a specific receiver geometry, such that the best image is obtained with the most practical (and cost efficient) source distribution.

Using Baseline Model 1 we can compute the theoretical surface source distribution and the virtual source CMP fold and offsets required to satisfy all the image rays (Figures 16 and 17). The computed surface source distribution consists of non equispaced source locations spread a distance of over 100 km from the borehole. The extent of this distribution is unrealistic to achieve by a walk-away VSP survey in practice. A realistic walk-away VSP survey source distribution would only extend a few hundred meters away from the borehole. This type of distribution would result in far-offset image rays being satisfied in preference to near offset image rays.

To determine the effect of a discrete source aperture on the virtual source CMP fold and offsets, we consider the same simplified hard rock scenario, this time with a walk-away source aperture of 1440 m (Table 1 – Model 1a). Figure 18 demonstrates that the effect of the discrete source aperture is to systematically remove the near-offset image rays from downhole CMPs. This implies that a near-offset filter should be applied to the virtual source CMP gathers prior to stack, to ensure that only the true virtual source information is included in the final image. If the noisy traces are included in the final stack then the signal to noise ratio of the downhole offsets will decrease, producing an increasingly distorted downhole image. Also note from Figure 18 that there is a downhole limit to the captured image rays. For this model the limit is CMP 520 which

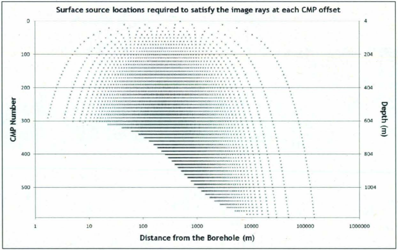

Figure 16. Surface Source Locations Required to Satisfy the Image Rays for Baseline Model 1.

Surface source locations required to satisfy the image rays at each CMP for Baseline Model 1 (Table 1). Note that the distance from the borehole is a log scale, and that the dataset has been decimated to each 10th CMP for clarity. For each CMP, far-offset traces require image rays generated by surface sources located close to the borehole, whereas near-offset traces require image rays generated by surface sources located far from the borehole. The sigmoidal-style cut-off of surface source locations deeper than CMP 300 is due to the combination of the walk-away VSP geometry failing to generate up-going image rays and that below CMP 300 the farthest offset is progressively removed.

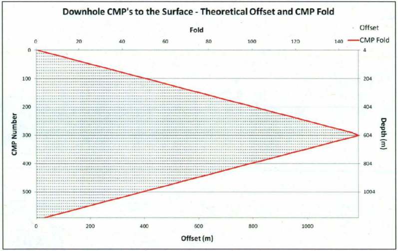

Figure 17. Theoretical Virtual Source CMP Offset and Fold for Baseline Model 1.

Theoretical fold and trace offset for each CMP location for the Baseline Model 1 (Table 1). For clarity the dataset has been decimated to every 10th CMP.

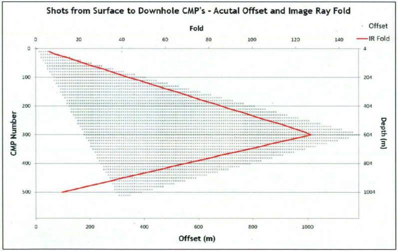

Figure 18. Actual Image Ray Offset and Fold for Model 1a.

The actual image rays offset and fold for each CMP location using the discrete source aperture as indicated in Table 1 (Model 1a). The near-offset image rays are progressively removed from downhole CMP's. For clarity the dataset has been decimated to every 10th CMP.

corresponds to a depth of 1044m. This means that for the last 160 m of the borehole we are not actually capturing any image rays.

3.4.3 Effect of Downhole Receiver Spacing

As noted earlier, the controlling factors affecting the geometry of the virtual source data are receiver number and spacing. Thus as well as ensuring the image rays are captured, it is important to consider whether the geometry of the virtual source survey is sufficient to image the target reflector. To address this issue the same simplified hard rock scenario was utilized, this time with 150 receivers spaced 8 m apart to a total depth of 1204 m (Figure 15, Table 1 – Baseline Model 2). The theoretical surface source distribution and virtual source CMP fold and offsets were then computed (Figures 19 and 20). This ray tracing analysis demonstrates that by halving the number of downhole receivers only half the number of virtual source CMP locations are imaged, which subsequently halves both the total number of shots required and the fold. This is not an especially surprising result, but does illustrate the importance of ensuring that the receiver number and spacing is adequate to generate the required virtual source CMP coverage and fold to image the target reflector.

The ray tracing analysis is used to determine the effects of a 1440 m discrete source aperture on the virtual source CMP fold and offsets (Table 1 – Model 2a). Figure 21

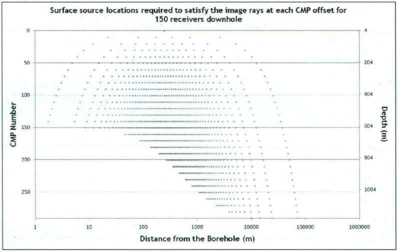

Figure 19. Surface Source Locations Required to Satisfy the Image Ray Geometry for Baseline Model 2.

Surface source locations required to satisfy the image rays at each CMP for Baseline Model 2 (Table 1). Note that the distance from the borehole is a log scale, and that the dataset has been decimated to each 10th CMP for clarity.

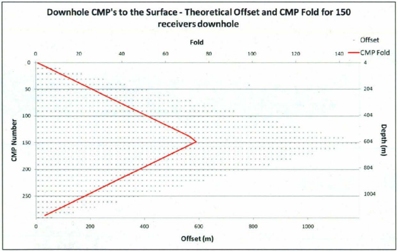

Figure 20. Theoretical Virtual Source CMP Offset and Fold for Baseline Model 2.

Theoretical fold and trace offset for each CMP location for the Baseline Model 2 (Table 1). For clarity the dataset has been decimated to every 10th CMP.

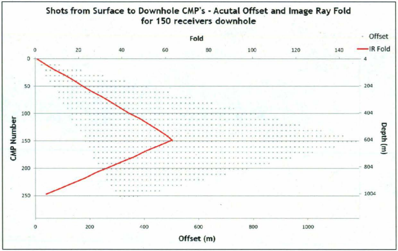

Figure 21. Actual Image Ray Offset and Fold for Model 2a.

The actual image ray offset and fold for each CMP location using the discrete source aperture as indicated in Table 1 (Model 2a). The near-offset image rays are progressively removed from downhole CMP's. For clarity the dataset has been decimated to every 10th CMP.

indicates the same progressive removal of downhole near-offset image rays as illustrated in Figure 18. This again implies that a near-offset filter should be applied to the virtual source data prior to stack to ensure spurious information does not degrade the final image. For this particular model Figure 21 also indicates that the image ray limit occurs at CMP 259 which corresponds to a depth of 1040 m. This means that for the last 164 m of the borehole no image rays are captured.

3.4.4 Effect of Reflector Location

Another important consideration is the location of the reflector from the borehole. The farther the reflector from the borehole, the farther the surface sources need to be to satisfy the required image rays (Figure 22). To quantify this observation the hard rock scenario was utilized again, this time with the vertical reflector located 500m from the borehole (Figure 15, Table 1 – Baseline Model 3). The theoretical surface source distribution and virtual source CMP fold and offsets were then computed (Figures 23 and 24). A comparison of Figure 16 and Figure 23 demonstrates that by increasing the reflector distance from the borehole the required surface source distribution is also shifted away from the borehole. Since none of the downhole receiver parameters have been changed the virtual source CMP fold and offsets are as per Baseline Model 1 (Compare Figure 17 and Figure 24). The major effect on the virtual source image ray fold and offsets is illustrated by Figure 25 which demonstrates the impact of the discrete source aperture of 1440 m (Table 1 – Model 3a). Comparison of Figure 25 and Figure 18 (which illustrates the affect on Model 1a) indicates that by increasing the distance of the reflector

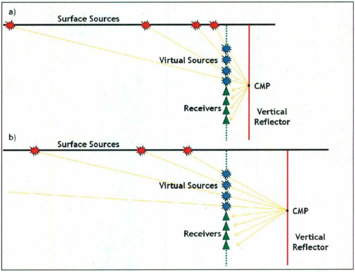

Figure 22. Virtual Source CMP for Difference Reflector Locations.

a) Several receiver pairs contribute to imaging a CMP location at the vertical reflector. Each receiver pair which contributes to the CMP location has a specific image ray geometry which is satisfied by a real surface source location. b) If the reflector is located farther from the borehole the effect is to also increase the distance of the required surface sources from the borehole. This indicates that the most efficient acquisition of walk-away VSP data for virtual source imaging will occur if the borehole is located close to the reflector.

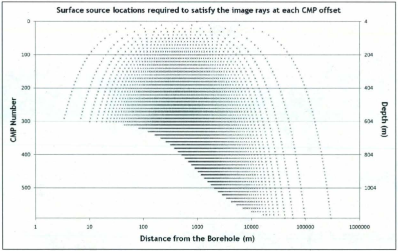

Figure 23. Surface Location of Sources required to Satisfy the Image Ray Geometry Baseline Model 3.

Surface source locations required to satisfy the image rays at each CMP offset for the Baseline Model 3 (Table 1). Note that the distance from the borehole is a log scale, and that the dataset has been decimated to each 10th CMP for clarity.

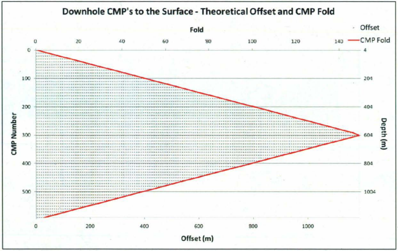

Figure 24. Theoretical Virtual Source CMP Offset and Fold for Baseline Model 3.

Theoretical fold and trace offset for each CMP location for the Baseline Model 3 (Table 1). For clarity the dataset has been decimated to every 10th CMP.

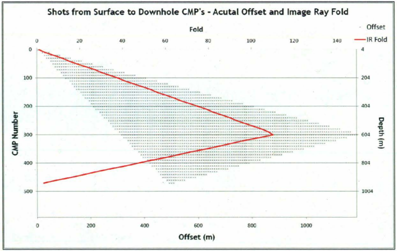

Figure 25. Actual Image Ray Offset and Fold for Model 3a.

The actual image ray offset and fold for each CMP location using the discrete source aperture as indicated in Table 1 (Model 3a). The near-offset image rays are progressively removed from downhole CMP's. For clarity the dataset has been decimated to every 10^{th} CMP.

from the borehole more of the near-offset image rays are removed more quickly down the borehole. This implies that an even more aggressive near-offset filter should be applied to the virtual source data. Finally we note that for this particular model the image ray limit occurs at CMP 259 which corresponds to a depth of 1040 m (Figure 25). This means that for the last 164 m of the borehole no image rays are captured.

3.5 Conclusions

The work presented in this Chapter has demonstrated that the virtual source method is valid despite violating the requirement that buried receivers be completely surrounded by surface sources, provided the source density is such that the incorrectly located events are sampled sufficiently, and the source aperture is broad enough to capture all the required image rays.

It has also been demonstrated that the geometry of the virtual source survey, including virtual source CMP fold and offset, is defined by the downhole receiver locations and spacing. And that source aperture, receiver spacing and reflector location have significant impact on the subsequent image ray fold and offset of the virtual source data. Thus care must be taken in understanding what the required image rays Geometry is and what image rays are actually captured by the walk-away VSP survey.

Finally we note that the walk-away VSP source distribution fails to generate an up-going image ray. That is, there are no virtual source contributions to receivers shallower than the virtual source under consideration, and as such only the downhole offsets in the virtual source CMP should utilized in generating the virtual source image.

Chapter 4 Generation of Virtual Source Data

4.1 Introduction

The process of generating virtual source data is simple; common receiver gathers are cross correlated for each source and then summed. Of course, as discussed in Chapter 3, correct application of the virtual source method requires both capture of the image ray and sufficient surface source sampling. The following is therefore a demonstration of how virtual source data is generated for a 2D synthetic model, and includes an analysis of the pre-stack CMP-sorted virtual source gathers and the final stacked and migrated virtual source image. To do so, a simple 250 m wide vertical dyke is imaged using a walk-away VSP acquisition geometry (Figure 26).

4.2 2D Synthetic Modelling

Synthetic generation of seismic data was performed in Seismic Unix using a 2nd order accurate acoustic finite difference algorithm. A walk-away VSP acquisition geometry was utilized to image the simple vertical dyke (Figure 26). The synthetic seismic response, generated by insertion of a zero phase Ricker wavelet into the discretized grid, was extracted along a vertical line within the model (Figure 27). The VSP acquisition geometry and the size and shape of the model were selected to compliment the work of Caddigan (2009) (Tables 2 and 3). The velocities and densities used for modeling were selected to reflect the seismic properties of a hard rock environment (Table 4). Specifically, for this research the seismic properties utilized were based on the country rock (granites and gneisses from the Reid Brook and Eastern Deep Zones) and mineral-bearing

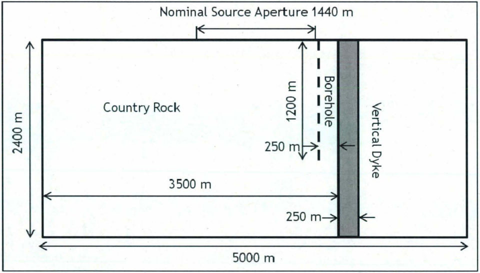

Figure 26. Geometry of the Vertical 2D Synthetic Model.

The 2D model is 5000 m wide and 2400 m high. The model is much larger than required in order to minimize the influence of edge effects.

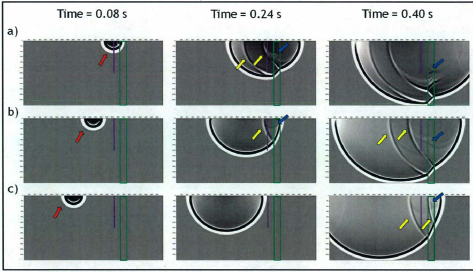

Figure 27. Snap Shot of the Wavefield Propagating Through the Baseline Model.

a) Shot 1 at 3236 m; b) Shot 90 at 2516 m; c) Shot 180 at 1796 m. The direct wave is highlighted by the red arrows. Reflections from the sides of the vertical dyke are indicated by the yellow arrows. Internal reflections within the dyke are identified by the blue arrows. The green box represents the location of the vertical dyke. The purple line is the location of the vertical line of receivers. Note: the tails off the primary reflections are head waves generated at the intersection of the top of the dyke and the free surface.

Table 2. 2D Model Parameters for the Simple Vertical Dyke.

The model parameters used for 2D synthetic modelling. Note that the total recorded time for all models was 0.6 seconds, decimated to a time increment of 1.0 ms.

***Signal to Noise ratio as determined by the Seismic Unix program suaddnoise.**

Model Name	Dyke Geometry	Velocity Model	Grid Model	Number of Shots	Shot Spacing (m)	Number of Receivers	Receiver Spacing (m)	Dominant Source Frequency (Hz)	Signal to Noise Ratio*
Baseline	Vertical	Homogeneous	4 m Model	180	8	300	4	40	1

Table 3. 2D Grid Parameters for the Simple Vertical Dyke.

Grid Parameters used for synthetic 2D modeling.

Grid Model	Grid Spacing (m)	Width (m)	Width – Number of Nodes	Height (m)	Height – Number of Nodes	Borehole Location (m)	Borehole Location – Node Number
2 m Model	2	5000	2500	2400	1200	3252	1626

Table 4. 2D Velocity and Density Model for the Simple Vertical Dyke.

Velocity Model	Dyke Velocity (m/s)	Dyke Density (kg/m^3)	Background Velocity (m/s)	Background Density (kg/m^3)	Velocity Gradient (s^{-1})	Percent Variation (%)	Approximate Hurst Number	Correlation Length (m)
Homogeneous	4500	4500	6300	2700	N/A	N/A	N/A	N/A

dykes (massive sulphides) encountered at the Voisey's Bay Mine (Duff, 2007). Refer to Appendix C for the code utilized to generate the data in Section 4.2.

4.3 Generating Virtual Source Data

Once synthetic data are generated, they are imported into ProMAX for initial analysis and quality control. A very broad (0-15-385-400 Hz) bandpass filter is applied to the data in order to remove very low and very high frequency numerical noise. The data are then exported and converted into Seismic Un*x format required by the process which generates the virtual source data. The processing sequence involves cross correlation of the recorded trace, at the location of the virtual source receiver, against the recorded trace, at the image receiver, and summation over all sources (Figure 28). Refer to Appendix D for the detailed processing sequence parameters and code used for generating the virtual source gathers. Once virtual source gathers are generated the data are imported into ProMAX for CMP sorting, NMO-correction, migration and stacking.

From Figure 28 we note that there is a character change between the events in the correlation gather (Figure 28e) (and virtual source trace (Figure 28d)) and the gathers (virtual source receiver and image receiver (Figures 28a and 28b)) from which these data are generated. This character change is typified by the direct wave, which for the virtual source data, appears zero-phase. For the VSP Receiver gathers however the event appears to be 90° phase. The virtual source direct wave is generated via the cross correlation

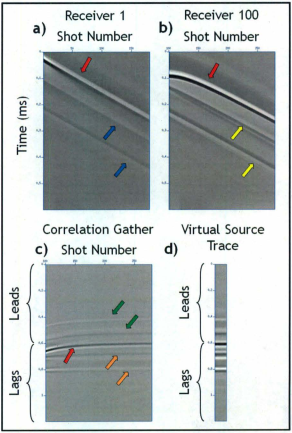

Figure 28. The Cross Correlation and Summation Process for Generating Virtual Source Data.

of the direct waves in the virtual source receiver and image receiver gathers. Provided the character of the direct waves in these gathers does not significantly change, this process is essentially an autocorrelation, which will result in the conversion of a 90° phase event into a zero phase event (Figure 29).

4.4 Analysis of Pre-Stack Virtual Source Data

First pass analysis of the CMP-sorted virtual source gathers demonstrates that direct interpretation of the data is not straightforward; the typical hyperbolic moveout of the reflection events is not evident, and several additional events with no apparent physical meaning are present (Figure 30b). In order to interpret better these events, a Forward model is used to generate data where the sources are coincident with the receivers (Figure 31, Tables 5 and 6). That is, this model represents what the virtual source method is attempting to achieve. Comparison of the virtual source data with that of the Forward model allows for increased understanding of the virtual source result (Figure 30a and 30b). The following is therefore an analysis of the pre-stack CMP-sorted virtual source gathers using the Forward model as a guide for interpretation.

Firstly we note a difference in the character of the seismic events between the Forward model and the virtual source data. This character difference is typified by the reflection event off the back of the dyke, which appears zero-phase in the virtual source data and 90° phase in the Forward model. This character difference was noted in the generation of the virtual source data as discussed in Section 4.3.

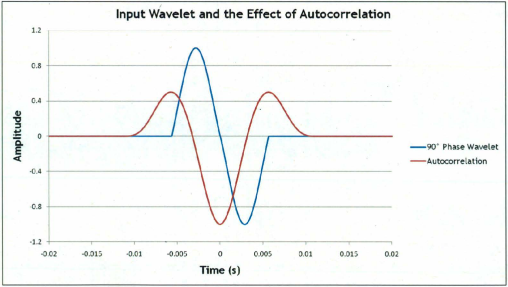

Figure 29. 90° Phase Wavelet and the Effect of Autocorrelation

The cross correlation process used to generate the virtual source data will fundamentally alter the shape of the seismic signal as illustrated by the autocorrelation of the input 90° phase wavelet.

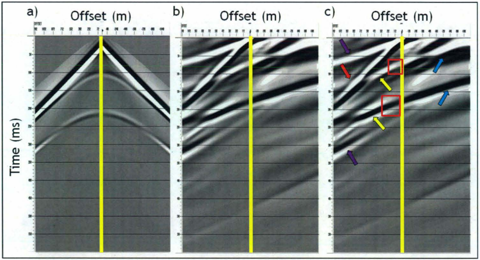

Figure 30. Comparison of Forward Model and Virtual Source Gathers at CMP 300.

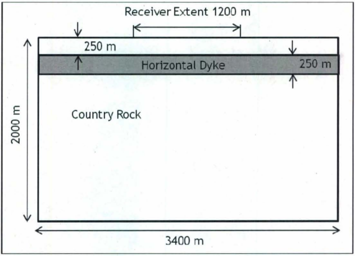

Figure 31. Geometry of the Forward Model.

The 2D model is 3400 m wide and 2000 m high. The model is much larger than required in order to minimize the influence of edge effects.

Table 5. Forward Model Parameters.

The model parameters used for 2D synthetic modeling of the Forward model. Note that the total recorded time for all models was 0.6 seconds, decimated to a time increment of 0.01ms.

***Signal to Noise ratio as determined by the Seismic Unix program suaddnoise.**

Model Name	Dyke Geometry	Velocity Model	Grid Model	Number of Shots	Shot Spacing (m)	Number of Receivers	Receiver Spacing (m)	Dominant Source Frequency (Hz)	Signal to Noise Ratio*
Forward	Horizontal	Homogeneous	4 m Model	300	4	300	4	40	1

Table 6. 2D Forward Model Grid Parameters.

Grid Parameters used for synthetic 2D modeling.

Grid Model	Grid Spacing (m)	Width (m)	Width – Number of Nodes	Height (m)	Height – Number of Nodes	First Shot / Receiver (m)	First Shot / Receiver – Node Number	Top of Dyke (m)	Top of Dyke – Node Number
4 m Model	4	3400	850	2000	500	1100	275	250	63

Next we note a time shift between the two datasets. This time shift is also due to the cross correlation process. As discussed in Section 4.3 the virtual source direct wave is generated via the cross correlation of the direct waves in the virtual source receiver and the image receiver gathers (Figure 28). The cross correlation process not only produces a phase change in the data, but it also locates the peak of the direct wave at zero time at zero offset. The Forward model on the other hand is generated by a synthetic modeling algorithm which locates zero time at zero offset at the onset of wavelet energy, not at the peak. This means we should expect a time shift in the virtual source data equal to the time of the peak of the wavelet in the Forward model. For this model the peak of the direct wave at zero offset is 28 ms, and we would therefore expect to see the virtual source data display a negative time shift of this magnitude. Figure 30b illustrates that this is the approximate time shift observed for the virtual source data.

As noted earlier, the typical hyperbolic moveout of the reflection events in not evident in the CMP-sorted virtual source gathers. This is a direct result of the observation in Chapter 3 that the VSP acquisition geometry does not generate any up-going image rays (Figure 13). This means the uphole offsets of the virtual source gather do not contain any image rays, and therefore the reflection events cannot properly characterize the typical moveout (Figure 30c).

Another key observation made in Chapter 3, was that a finite source aperture will progressively remove near-offset image rays from downhole CMP's (Section 3.4). This is manifest in the reflection events as incorrect positioning and a decrease in amplitude at near-offsets (Figure 30c). This provides further evidence that for this particular hard rock scenario, a near-offset filter should be applied to the CMP-sorted virtual source gathers prior to stack to ensure that only correctly located data is included in the final image.

The final observation to make of the CMP-sorted virtual source gathers is that several events with no apparent physical meaning are present in the data (Figure 30c). This is a direct effect of the finite source aperture and has been highlighted by Mehta et al. (2008) and Schuster (2009). These non-physical events are generated by the cross correlation process and would be fully cancelled by the summation process if the buried receivers were completely surrounded by sources. Since practical implementation requires a finite source aperture these events are not fully destroyed by the interference process. As per the mathematical analogies discussed in Section 3.3, this is due to the truncation of the integration limits (ie. the finite source aperture) with the result being that the edges of the cross correlation event stack into the virtual source data.

4.5 Analysis of the Virtual Source Stack

In order to generate the virtual source stack the CMP-sorted virtual source gathers are NMO-corrected using a constant velocity field of 6300 m/s. The NMO-corrected CMP gathers are then stacked and migrated using the Stolt F-K migration algorithm with a constant velocity field of 6300 m/s. The final virtual source stack images the front and the back of the dyke well, except at the very bottom of the borehole, where the amplitudes of the reflection events are dimmed and the positioning is incorrect (Figure 32a).

Recall that in Section 4.4 several key observations were made regarding the effects of the walk-away VSP acquisition geometry on the CMP-sorted virtual source gathers. The first was that surface sources fail to generate an up-going image ray, such that the expected hyperbolic moveout is not observed for uphole offsets. This observation suggests that only the downhole offsets for a particular virtual source CMP should be stacked into the final image. A comparison of the final migrated stacks, one using all offsets, the other only downhole offsets, demonstrates that by stacking in only the downhole offsets we can produce a final image with better amplitude fidelity (Figure 32a and 32b). We note however, that the positioning of the reflection events is still poor at the bottom of the borehole.

Another key observation in Section 4.4 was that the near-offset traces suffered from incorrect positioning and a decrease in amplitude due to the progressive removal of near-offset image rays from downhole CMP's (Figure 30c). This implies that a near-offset filter should be additionally applied to the CMP-sorted virtual source gathers prior to stack to ensure that only data actually containing image rays be stacked into the final image. Using the results from the ray tracing analysis in Section 3.4 a near-offset filter is derived to image optimally both the front and back of the dyke. It is clear from Figures 32c and 32d that use of the near-offset filters results in the correct kinematic

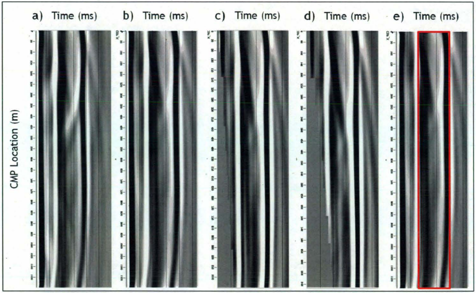

Figure 32. Virtual Source Stacks for the Baseline Model.

a) Virtual source stack generated from all virtual source traces; b) The virtual source stack generated using downhole offsets; c) The virtual source Stack generated using the near-offset filter; d) The virtual source stack generated using the more aggressive near-offset filter to image optimally the back reflector; e) The virtual source stack with the dyke indicated in red.

positioning of both the front and back of the dyke, in additional to providing good amplitude fidelity for the length of the reflection events.

4.6 Conclusions

The work in this Chapter demonstrated that virtual source data is generated via a cross correlation and summation process. Analysis of the pre-stack CMP-sorted virtual source gathers resulted in the identification of several features caused by the cross correlation process. These include a fundamental change in the character of the seismic events, and a time shift in the data such that time zero corresponds to the peak of the direct wave energy, not the onset.

The analysis of the pre-stack gathers also highlighted features associated with the finite source aperture, such as the non-hyperbolic moveout of the uphole offsets, incorrect positioning and a decrease in amplitude of the reflection events at near offsets, and the presence of several events with no apparent physical meaning. Understanding these features allows for an optimal final virtual source image to be generated.

Chapter 5 Practical Implementation of the Virtual Source Method

5.1 Introduction

The ultimate aim of this study is to understand the acquisition and processing parameters required to image steeply dipping features in a hard rock environment using the virtual source method. In Chapter 3 it was proven via a ray tracing analysis that the virtual source method is capable of producing the correct kinematic image despite a finite source aperture. The analysis also highlighted the importance of capturing the image ray and the effects of varying acquisition parameters such as receiver spacing and distance of the borehole from the reflector. Chapter 4 demonstrated the process for generating a virtual source image and again highlighted the importance of ensuring only the data containing image rays are stacked into the final image. The following is therefore a discussion of the practical implementation issues associated with ensuring correct application of the virtual source method for several different walk-away VSP geometries and velocity and density fields. Two geometries are analyzed, the first consists of the simple 250 m wide vertical dyke (Figure 26). Perfectly vertical features are geologically rare, so to test the ray-tracing analysis further a more realistic model of the steeply dipping feeder dyke is utilized (Figure 33).

5.2 2D Synthetic Modelling

Seven models with differing acquisition parameters (Tables 7, 8 and 9) were utilized. Four other models with heterogeneous velocity and density fields (Tables 7, 8 and 9, Figures 34, 35 and 36) were utilized in order to address additional issues highlighted in the geophysical literature. These issues are the ability of turning waves and scattered waves to generate seismic energy with broader angles of incidence than that generated by the actual surface source aperture. By broadening the angles of incidence the heterogeneous earth structure is in effect creating new image rays, therefore potentially improving both the extent and quality of the virtual source image (refer to Section 5.2.1).

As per Chapter 4, synthetic generation of seismic data was performed in Seismic Unix using a 2nd order accurate acoustic finite difference algorithm. A walk-away VSP acquisition geometry was utilized to image both the simple vertical dyke (Figure 26) and the more realistic feeder dyke geometry (Figure 33). The synthetic seismic response, generated by insertion of a zero phase Ricker wavelet into the discretized grid, was extracted along a vertical line within the model (Figure 37). The VSP acquisition geometry and the size and shape of both models were selected to complement the work of Caddigan (2009) (Tables 7 and 8). The velocities, densities, velocity gradients and percent velocity/density variations used for the modeling were selected to reflect the seismic properties of a hard rock environment. Specifically, for this research the seismic properties utilized were based on the country rock (granites and gneisses from the Reid Brook and Eastern Deep Zones) and mineral-bearing dykes (massive sulphides) encountered at the Voisey's Bay Mine (Duff, 2007) (Table 9). Refer to Appendix C for the code utilized to generate the data in Section 5.2.

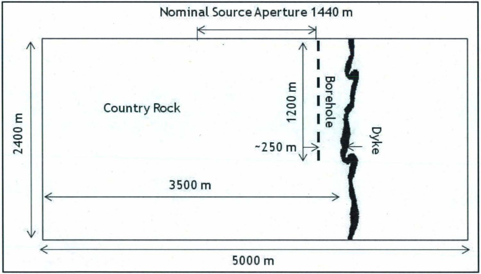

Figure 33. Geometry of the Complex 2D Synthetic Model.

The 2D model is 5000 m wide and 2400 m high. The model is much larger than required in order to minimize the influence of edge effects

Table 7. 2D Model Parameters.

The model parameters used for 2D synthetic modelling. Note that the total recorded time for all models was 0.6 seconds, decimated to a time increment of 0.01ms. Values varying from Baseline Model 1 are highlighted in gray.

***Signal to Noise ratio as determined by the Seismic Unix program suaddnoise.**

Model Name	Dyke Geometry	Velocity Model	Grid Model	Number of Shots	Shot Spacing (m)	Number of Receivers	Receiver Spacing (m)	Dominant Source Frequency (Hz)	Signal to Noise Ratio*
Baseline	Vertical	Homogeneous	4 m Model	180	8	300	4	40	1
Complex Baseline	Complex	Homogeneous	4 m Model	180	8	300	4	40	90
Complex 90 Shot	Complex	Homogeneous	4 m Model	90	16	300	4	40	90
Complex 45 Shot	Complex	Homogeneous	4 m Model	45	32	300	4	40	90
Complex 40 Shot 40 Hz	Complex	Homogeneous	2 m Model	40	60	300	4	40	90
Complex 40 Shot 80 Hz	Complex	Homogeneous	2 m Model	40	60	300	4	80	90
Gradient Model 1	Vertical	Gradient Model 1	4 m Model	180	8	300	4	40	1
Gradient Model 2	Vertical	Gradient Model 2	4 m Model	180	8	300	4	40	1
Gaussian Random	Vertical	Gaussian Random	4 m Model	180	8	300	4	40	1
Two-Phase Random	Vertical	Two-Phase Random	4 m Model	180	8	300	4	40	1

Table 8. 2D Grid Parameters.

Grid Parameters used for synthetic 2D modeling.

Grid Model	Grid Spacing (m)	Width (m)	Width – Number of Nodes	Height (m)	Height – Number of Nodes	Borehole Location (m)	Borehole Location – Node Number
2 m Model	2	5000	2500	2400	1200	3252	1626
4 m Model	4	5000	1250	2400	600	3252	813

Table 9. 2D Velocity and Density Models.

The velocity and density models increase in complexity and inhomogeneity.

***The velocity gradient in Gradient Model 2 was intended to reflect the velocity gradients encountered a typical Tertiary sedimentary basin (Haskell, 1941).**

Note the Hurst number quantifies the self-similarity of the medium that is, it is a measure of the complexity or roughness of the medium. The correlation length represents the longest scale at which the medium is truly self-similar.

Velocity Model	Dyke Velocity (m/s)	Dyke Density (kg/m^3)	Background Velocity (m/s)	Background Density (kg/m^3)	Velocity Gradient (s^{-1})	Percent Variation (%)	Approximate Hurst Number	Correlation Length (m)
Homogeneous	4500	4500	6300	2700	0.000	N/A	N/A	N/A
Gradient Model 1	4500	4500	6300	2700	0.170	N/A	N/A	N/A
Gradient Model 2*	4500	4500	6300	2700	0.464	N/A	N/A	N/A
Gaussian Random	4500	4500	5900	2700	0.000	3	0.3	150
Two-Phase Random	4500	4500	5900	2700	0.000	3	0.3	150

5.2.1 2D Synthetic Modelling with Heterogeneous Velocity and Density Fields

Many of the petroleum applications of the virtual source method rely on strong velocity gradients associated with compacted sedimentary sequences. These strong velocity gradients induce turning waves which can illuminate hard to image features such as salt-dome overhangs and can allow for the capture of up-going image rays. In order to determine the importance of these turning waves for a hard rock scenario, two velocity gradient models were studied, one with a gradient typical of the country rock at Voisey's Bay mine (Gradient Model 1, Figure 37b), and the other intended to reflect a typical velocity gradient encountered in a petroleum style environment (Gradient Model 2, Figure 37c).

As seismic energy propagates through random heterogeneous media, secondary waves are generated at the site of local heterogeneities (Aki and Chouet, 1975). These scattered waves are of particular interest to those utilizing the virtual source method as this energy has been demonstrated to increase the effective imaging aperture (Bakulin and Calvert, 2006). These studies however have been conducted for petroleum models and not for the hard rock model that is that being considered in this study.

Random heterogeneous media used in synthetic modeling is generated by the addition of two components; a small component of random, spatially distributed velocity and density

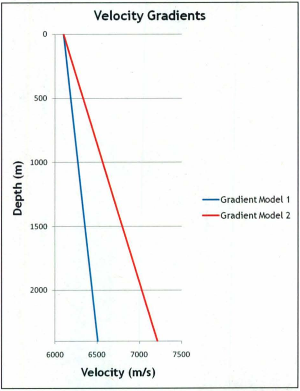

Figure 34. Velocity Gradients.

Gradient Model 1 (blue line) has a velocity gradient of 0.170 as encountered in the country rock at Voisey's Bay mine. Gradient Model 2 (red line) has a velocity gradient of 0.464, which is a typical petroleum environment velocity gradient. Note the density model for these models is constant as per the Baseline model (Tables 7, 8 and 9).

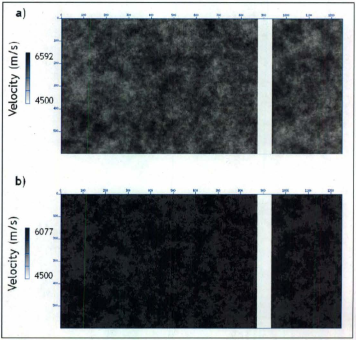

Figure 35. **Heterogeneous Velocity Models.**

a) Gaussian Random model; b) Two Phase model. The dyke velocity is held constant at 4500 m/s and does not vary internally. Note that the horizontal and vertical scale is in grid nodes.

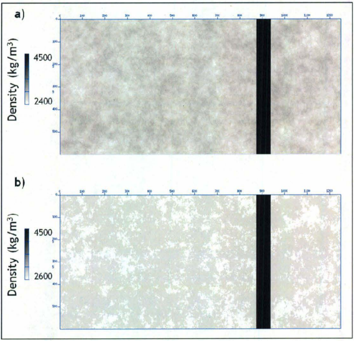

Figure 36. Heterogeneous Density Models.

a) Gaussian Random model; b) Two Phase model. The dyke density is held constant at 4500 kg/m^3 and does not vary internally. Note that the horizontal and vertical scale is in grid nodes.

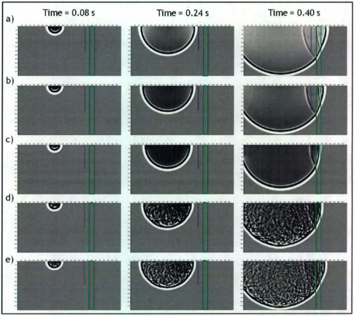

Figure 37. Snap Shot of Propagating Wavefield for Shot 180 at 1796 m.

a) Baseline model; b) Gradient Model 1; c) Gradient Model 2; d) Gaussian Random model; e) Two Phase model. The green box represents the location of the vertical dyke. The purple line is the location of the vertical line of receivers.

values superimposed onto a distribution of average values (Frankel and Clayton, 1986). Two end member models are used to address the effects of a scattering media on the imaging abilities of the virtual source method. The Gaussian Random model uses a von Karman autocorrelation function to generate smoothly-varying, spatially-distributed, fractal-patterned velocity and density values superimposed onto a Gaussian velocity and density distribution (Figure 37d). The Two Phase Random model uses the same spatial distribution of velocity and density values, but instead these values are superimposed onto a two-phase end-member velocity and density distribution (Figure 37e). These random models also represent geological end members. Due to the abrupt velocity and density contrasts of the Two Phase Random model, this model is expected to provide the most scattering and therefore have the highest likelihood of increasing the effective imaging aperture in a hard rock model.

5.3 Imaging a Vertical Feature with Complex Geometry

As discussed earlier perfectly vertical features are geologically rare, so to test the ray-tracing analysis further a more realistic model of the steeply dipping feeder dyke is utilized (Figure 33). In order to generate the virtual source stack the CMP-sorted virtual source gathers are NMO-corrected using a constant velocity field of 6300 m/s. The NMO-corrected CMP gathers are then stacked and migrated using the Stolt F-K migration algorithm, using the constant velocity field of 6300 m/s. A comparison of the final stacks using all offsets (Figure 38a), downhole offsets (Figure 38b) and the offsets that pass the near-offset filter (Figure 38c) confirms the conclusion in Chapter 4, that it is important to ensure only the true image rays are stacked into the final image. Also it is clear that the

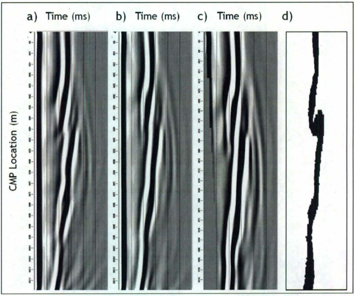

Figure 38. Virtual Source Stack of the Complex Model.

a) Virtual source stack generated from all virtual source traces. b) The virtual source stack generated using downhole offsets. c) The virtual source stack generated using the near-offset filter. d) The geometry of the complex dyke being imaged by the virtual source stack.

virtual source method is a viable technique for imaging vertical subsurface features with complex geometries.

5.4 Extending the Effective Source Aperture

The model we considered in Chapter 4 consisted of a homogeneous velocity and density field. The earth however is far from homogeneous. Therefore a more realistic model will utilize a heterogeneous field. Additionally, as discussed in Section 5.2, heterogeneous velocity and density fields have the potential to improve the virtual source image by extending the effective source aperture. Up-going image rays in particular are needed to characterize properly the typical hyperbolic moveout (Section 4.4). Turning waves generated by gradient velocity fields have the ability to produce up-going image rays. Turning rays are especially important in petroleum applications for imaging overhanging features, such as the underside of salt-domes. They are also most effective for imaging features several kilometers below the surface. Therefore it is not necessarily expected that turning waves will have a significant impact for a shallow hard rock application. Gradient Model 1 and Gradient Model 2 demonstrate that the reflection events for the uphole offsets do not display the typical hyperbolic moveout expected for a gradient velocity field (Figure 39b and 39c). This confirms our expectation that gradient velocity fields will have little impact for hard rock virtual source applications.

Scattering waves in heterogeneous media have also been proven to increase the effective imaging aperture (Bakulin and Calvert, 2006) by generating up-going image rays.

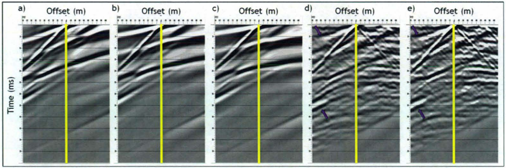

Figure 39. Virtual Source Gathers at CMP 300.

a) Baseline model. b) Gradient Model 1. c) Gradient Model 2. d) Gaussian Random model. e) Two-Phase Random model.

Zero offset is indicated by the yellow line. Downhole offsets (to the left of the zero offset), which are generated from data containing image rays, contain correctly located direct waves and reflected events. Uphole offsets (to the right of the zero offset) are generated from data which should not contain image rays unless they are created by scattered seismic waves. Note the weak direct waves evident in models 10 and 11 (panels d) and e)) due to the scattered waves generating some up-going seismic energy. Note spurious events due to the finite source aperture (indicated by the purple arrows) are weaker in the scattering models.

We address this issue by studying the impact of a Gaussian Random and Two-Phase Random velocity and density fields (Section 5.2.1) on the pre-stack CMP-sorted virtual source data. Figures 39d and 39e demonstrate that the heterogeneous models do produce enough back-scatter to extract the direct wave from the uphole offsets. Unfortunately for these models, the scattering is insufficient to produce uphole reflection events. This is disappointing as it was hoped that the heterogeneous nature of the earth would aid the virtual source imaging process. In terms of the practical implementation of the virtual source method, this observation suggests that for this particular hard rock scenario, even for extremely heterogeneous velocity and density fields, no uphole offsets should be stacked into the final virtual source image.

We do note however that an unexpected impact of the random heterogeneous media is to reduce the presence of non-physical events in the CMP-sorted virtual source gathers (Figures 39d and 39e). It appears that the scattered energy perturbs the non-stationary phase contributions enough to ensure more effective cancelation of these events. This is expected to be a benefit in terms of real data acquisition, as the heterogeneous nature of the earth will result in a virtual source image suffering from less contamination from non-physical events.

5.5 Surface Source Spacing

In terms of the practical acquisition of the any seismic data, surface source distribution is an extremely important consideration especially in the context of economic and environmental impact. If the total number of shots can be reduced, then the environmental impact will be lessened as will the cost of acquiring the survey. From the ray tracing analysis undertaken in Chapter 3 it is clear that source spacing is a critical aspect of ensuring correct application of the virtual source method. In particular, sufficient source spacing is necessary to ensure satisfactory interference of the non-stationary phase contributors. This issue was examined in Section 3.3 with a rudimentary demonstration of the importance of sufficient sampling, however to date we have yet to consider the bandlimited nature of seismic waves and the impact on source spacing and effective interference. Refer to Appendix E for the Fortran code utilized to generate the data in Section 5.4.

Mehta et al. (2008) noted that the effectiveness of the destructive interference of adjacent non-stationary phase contributions is dependent on the slope of the event in the cross correlation gather. This slope is equal to the difference between arrival times of the pulses in two adjacent traces, and the spacing between the surface sources. This relationship means that if the pulse arrivals are closer together then the surface source spacing can be coarser. Factors that influence pulse arrivals include receiver spacing, wavefield velocity, receiver depth, reflector location and angles of incidence and reflection (Mehta et al., 2008). The survey geometry considered by Mehta et al. (2008) consisted of horizontally-oriented receivers buried below a complex heterogeneous overburden for the purpose of imaging a horizontal subsurface feature. The walk-away VSP geometry utilized for this study is significantly different from this horizontal geometry, thus an independent analysis of the impact of the survey variables on the pulse arrivals is necessary.

To address this issue for a walk-away VSP survey, the simplified hard rock model is again utilized (Figure 15). Different VSP geometries and velocities are modelled in order to understand the relative effects of reflector location, velocity, receiver and source spacing on the time difference between the pulse arrivals in the cross correlation gather (Table 10). A simple ray tracing process determines the time difference between the direct and reflected events at a specific receiver pair in order to simulate the cross correlation process. From this simulated cross correlation gather, the time difference between adjacent pulses can be computed (Figure 40). This time difference is important as we require adjacent pulses to be below the Ricker's Criterion (Kallweit and Wood, 1982) of the peak frequency (f_P) of the pulse in order to apply properly stationary phase theory (Section 3.3) (Figures 41 and 42). That is, we require pulses to be offset by less than the temporal resolution (T_R) (as defined by Ricker's Criterion) to ensure effective destruction of the non-stationary phase contributions, where;

$$T_R = \frac{1}{3.0 \times f_P}$$

Equation 1. Ricker's Criterion

For the different models we extract the time difference between adjacent shot locations within the correlation gather for several receiver pairs (Figures 43 through 48). By cross plotting these time differences against the surface source locations we can graphically represent the range of time differences present in the correlation gathers at a particular virtual source for several receiver pairs. Figure 43 demonstrates that the range of time differences for the Baseline model (Table 10) is below ± 0.0012 s. This is well below the Ricker's Criterion for both a 40 Hz (0.00833 s) and an 80 Hz (0.00416 s) Ricker wavelet. This suggests that for the hard rock model under consideration, a source spacing of 8 m is sufficiently dense to ensure effective destruction of the non-stationary phase contributions. Figures 44, 45 and 46 demonstrate the impact of velocity, receiver spacing and reflector distance respectively on the range of time differences in the correlation gather. It is clear that the relative impact of these variables on the calculated time differences is minimal. Figures 47 and 48 however indicate that source spacing has a much larger relative impact on the range of time differences. The range of time differences for Source Spacing Model 1 (16 m source spacing) is ± 0.0021 s, and for Source Spacing Model 2 (32 m source spacing) is ± 0.0037 s. Again however these ranges are well below the Ricker's Criterion for both the 40 Hz and 80 Hz wavelet. This therefore suggests for the Baseline hard rock model a source spacing of 32 m is sufficient to ensure correct application of the virtual source method.

Complex, Complex 90 Shot and Complex 45 Shot (Table 7) are 2D synthetic models generated in Seismic Unix using a 40 Hz Ricker wavelet for a constant source aperture of 1440 m, with total shots of 180, 90 and 45 respectively. This corresponds to a source spacing of 8 m, 16 m and 32 m. Comparison of the final virtual source stacks for these models (Figure 49) indicates almost no difference between the final images. This

Table 10. Ray Tracing Models for Source Spacing Analysis.

Parameters are varied in the ray tracing models in order to understand better the source spacing for generating virtual source data. Parameters are defined in Figure 15. Values varying from the Baseline model are highlighted in gray.

Model		Source Aperture (S m)	Source Spacing (Y m)	Total Number of Sources	Receiver Spacing (R m)	Number of Receivers (M)	Reflector distance from Borehole (X m)	Wavefield Velocity (m/s)
Number	Name							
1	Baseline	1440	8	180	4	300	250	6300
2	Velocity	1440	8	180	4	300	250	4500
3	Receiver Spacing	1440	8	180	8	150	250	6300
4	Reflector Distance	1440	8	180	4	300	500	6300
5	Source Spacing 1	1440	16	90	4	300	250	6300
6	Source Spacing 2	1440	32	45	4	300	250	6300
7	Source Spacing 3	2400	60	40	4	300	250	6300

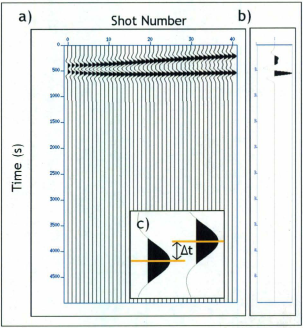

Figure 40. Simulated Correlation Gather.

a) The simulated correlation gather computed for model 1. Note only the cross correlated direct and reflected events are computed; b) The corresponding virtual source trace; c) The time difference between adjacent traces in the correlation gather.

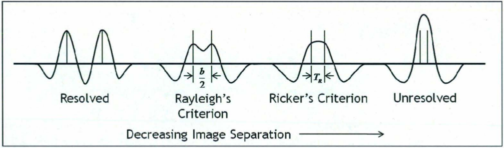

Figure 41. **Ricker's Resolution Criterion.**

To ensure effective destructive interference of the non-stationary phase contributors in the correlation gather, the time difference between adjacent traces must be below the Ricker's Criterion for Resolution, T_R. T_R is defined as $(3.0*f_P)^{-1.0}$, where f_P is equal to the peak frequency of the Ricker wavelet spectrum. After Kallweit and Wood, 1982.

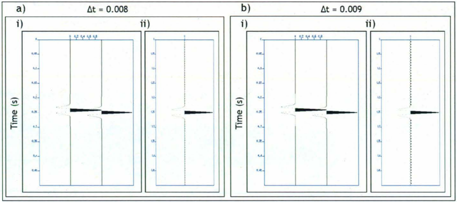

Figure 42. Effective Destructive Interference of Non-Stationary Phase Contributions.

The Ricker Wavelet examined here has a peak frequency of 40 Hz, which corresponds to a temporal resolution, as defined by Ricker's Criterion, of 0.008333 s

a) For the entire length of the record, the 40 Hz Ricker wavelets are summed together separated by a time difference of $\Delta t = 0.008$ s which is *below* the temporal resolution for this frequency: i) The spacing between two adjacent Ricker Wavelets; ii) The result of the summation process. It is clear that for a time difference of $\Delta t = 0.008$ s we obtain effective destructive interference of the non-stationary phase contributions.

b) For the entire length of the record, the 40 Hz Ricker wavelets are summed together separated by a time difference of $\Delta t = 0.009$ s which is *above* the temporal resolution for this frequency: i) The spacing between two adjacent Ricker Wavelets; ii) The result of the summation process. It is clear that for a time difference of $\Delta t = 0.009$ s we do not obtain effective destructive interference of the non-stationary phase contributions.

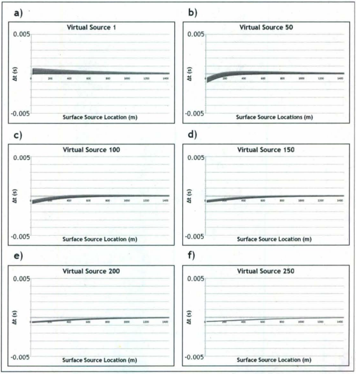

Figure 43. Time Difference Range for Baseline Model.

Time difference between the peak of adjacent pulses for the reflection event in the simulated correlation gather for a) Receiver pairs for virtual source 1 and every 10th image receiver from 2 to 300; b) Receiver pairs for virtual source 50 and every 10th image receiver from 51 to 300; c) Receiver pairs for virtual source 100 and every 10th image receiver from 101 to 300; d) Receiver pairs for virtual source 150 and every 10th image receiver from 151 to 300; e) Receiver pairs for virtual source 200 and every 10th image receiver from 201 to 300; f) Receiver pairs for virtual source 250 and every 10th image receiver from 251 to 300.

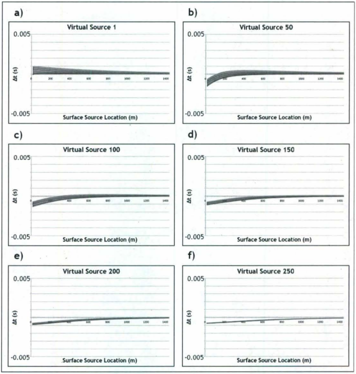

Figure 44. Time Difference Range for Velocity Model.

Time difference between the peak of adjacent pulses for the reflection event in the simulated correlation gather for a) Receiver pairs for virtual source 1 and every 10th image receiver from 2 to 300; b) Receiver pairs for virtual source 50 and every 10th image receiver from 51 to 300; c) Receiver pairs for virtual source 100 and every 10th image receiver from 101 to 300; d) Receiver pairs for virtual source 150 and every 10th image receiver from 151 to 300; e) Receiver pairs for virtual source 200 and every 10th image receiver from 201 to 300; f) Receiver pairs for virtual source 250 and every 10th image receiver from 251 to 300.

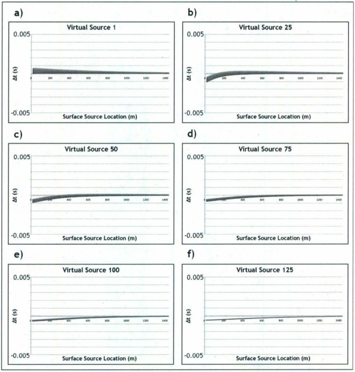

Figure 45. Time Difference Range for Receiver Spacing Model.

Time difference between the peak of adjacent pulses for the reflection event in the simulated correlation gather for a) Receiver pairs for virtual source 1 and every 10th image receiver from 2 to 300; b) Receiver pairs for virtual source 50 and every 10th image receiver from 51 to 300; c) Receiver pairs for virtual source 100 and every 10th image receiver from 101 to 300; d) Receiver pairs for virtual source 150 and every 10th image receiver from 151 to 300; e) Receiver pairs for virtual source 200 and every 10th image receiver from 201 to 300; f) Receiver pairs for virtual source 250 and every 10th image receiver from 251 to 300.

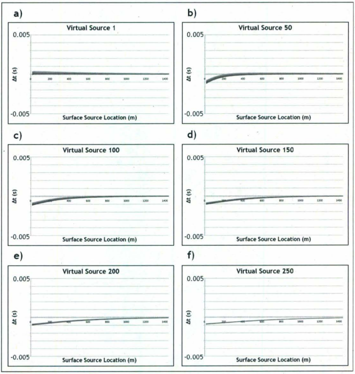

Figure 46. Time Difference Range for Reflector Distance Model.

Time difference between the peak of adjacent pulses for the reflection event in the simulated correlation gather for a) Receiver pairs for virtual source 1 and every 10th image receiver from 2 to 300; b) Receiver pairs for virtual source 50 and every 10th image receiver from 51 to 300; c) Receiver pairs for virtual source 100 and every 10th image receiver from 101 to 300; d) Receiver pairs for virtual source 150 and every 10th image receiver from 151 to 300; e) Receiver pairs for virtual source 200 and every 10th image receiver from 201 to 300; f) Receiver pairs for virtual source 250 and every 10th image receiver from 251 to 300.

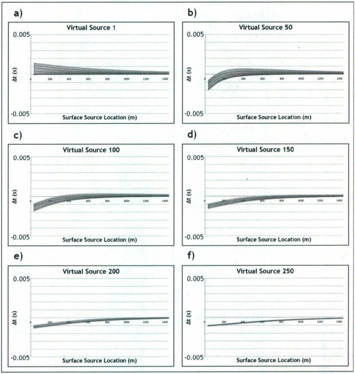

Figure 47. Time Difference Range for Source Spacing 1 Model.

Time difference between the peak of adjacent pulses for the reflection event in the simulated correlation gather for a) Receiver pairs for virtual source 1 and every 10th image receiver from 2 to 300; b) Receiver pairs for virtual source 50 and every 10th image receiver from 51 to 300; c) Receiver pairs for virtual source 100 and every 10th image receiver from 101 to 300; d) Receiver pairs for virtual source 150 and every 10th image receiver from 151 to 300; e) Receiver pairs for virtual source 200 and every 10th image receiver from 201 to 300; f) Receiver pairs for virtual source 250 and every 10th image receiver from 251 to 300.

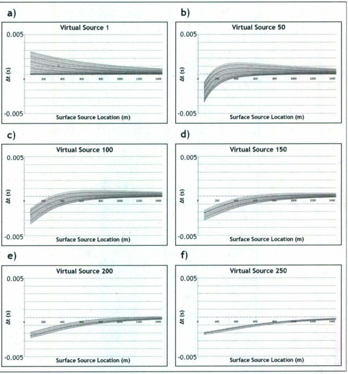

Figure 48. Time Difference Range for Source Spacing 2 Model.

Time difference between the peak of adjacent pulses for the reflection event in the simulated correlation gather for a) Receiver pairs for virtual source 1 and every 10^{th} image receiver from 2 to 300; b) Receiver pairs for virtual source 50 and every 10^{th} image receiver from 51 to 300; c) Receiver pairs for virtual source 100 and every 10^{th} image receiver from 101 to 300; d) Receiver pairs for virtual source 150 and every 10^{th} image receiver from 151 to 300; e) Receiver pairs for virtual source 200 and every 10^{th} image receiver from 201 to 300; f) Receiver pairs for virtual source 250 and every 10^{th} image receiver from 251 to 300.

confirms the conclusions drawn from the ray tracing analysis that the time differences in the correlation gather are much smaller than the Ricker's Criterion for the 40 Hz wavelet.

To test the impact of violating Ricker's Criterion in the correlation gather, another model is considered, Source Spacing 3 (Table 10, Figure 50). This model utilizes the same acquisition set-up as the Baseline model, however the source aperture is 2400 m and consists of 40 shots at 60 m spacing. The time difference range in the correlation gather is much broader than any of the other models considered so far. This is expected as it was previously concluded that source spacing has a much bigger relative impact on the time difference range than any other parameter. From Figure 50 we note that for a 40 Hz wavelet, the model will be below the Ricker's Criterion, however for an 80 Hz wavelet, some elements of the time difference range for the correlation gather are above the Ricker's Criterion. This indicates that we should not expect total effective destruction of the non-stationary phase contributions for seismic data generated with an 80 Hz Ricker wavelet. This is confirmed by Complex 40 Shot 40 Hz and Complex 40 Shot 80 Hz 2D synthetic models (Table 7). Comparison of the final virtual source stacks for these models (Figure 51) indicates that the Complex 40 Shot 80 Hz final image is blurred compared to the Complex and Complex 40 Shot 40 Hz final images. This confirms the conclusions drawn from the ray tracing analysis that it is critical that the time differences in the correlation gather be below the Ricker's Criterion, for the peak frequency of the wavelet in the recorded seismic data, to ensure effective destructive interference of the non-stationary phase contributions.

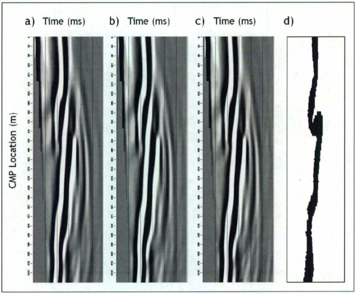

Figure 49. Virtual Source Stack of the Complex, Complex 90 Shot and Complex 45 Shot Models.

a) Complex model. b) Complex 90 Shot model. c) Complex 45 Shot model. The increasing source spacing does not affect the final virtual source image. This is because the time differences in the correlation gather for each model are much smaller than the Ricker's Criterion for the 40 Hz wavelet.

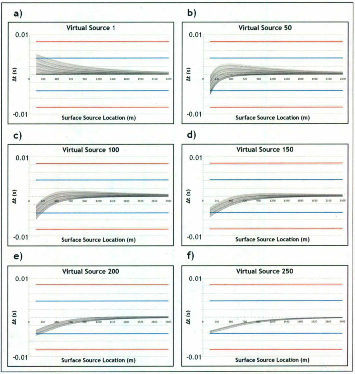

Figure 50. Time Difference Range for Source Spacing 3 Model.

Time difference between the peak of adjacent pulses for the reflection event in the simulated correlation gather for a) Receiver pairs for virtual source 1 and every 10th image receiver from 2 to 300; b) Receiver pairs for virtual source 50 and every 10th image receiver from 51 to 300; c) Receiver pairs for virtual source 100 and every 10th image receiver from 101 to 300; d) Receiver pairs for virtual source 150 and every 10th image receiver from 151 to 300; e) Receiver pairs for virtual source 200 and every 10th image receiver from 201 to 300; f) Receiver pairs for virtual source 250 and every 10th image receiver from 251 to 300. Note that the Ricker's Criterion for a 40 Hz wavelet is indicated in red and for an 80 Hz wavelet is indicated in blue.

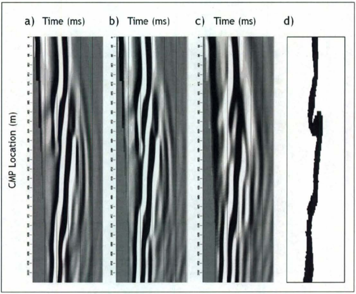

Figure 51. Virtual Source Stack of the Complex, Complex 40 Shot 40 Hz and Complex 40 Shot 80 Hz Models.

a) Complex model. b) Complex 40 Shot 40 Hz model. c) Complex 40 Shot 80 Hz model. By increasing the peak source frequency from 40 Hz to 80 Hz, the temporal resolution is increased from 0.00833 s to 0.00416 s. According to the time difference analysis (Figure 50) the 60 m source spacing model is below the Ricker's Criterion for the 40 Hz model and sections of the data are above the Ricker's Criterion for the 80 Hz model. There is a significant decrease in the quality of the virtual source image for the 80 Hz model over the 40 Hz model. Note that the 80 Hz model has been bandpass filtered to the same frequency content as the 40 Hz model.

5.6 Conclusions

The work presented in this Chapter has demonstrated several practical implementation issues, including the impact of heterogeneous velocity and density fields, the ability of the virtual source method to image vertical features with complex geometries, and the importance of surface source spacing on ensuring effective destructive interference of the non-stationary phase contributions.

It was demonstrated that heterogeneous velocity and density fields are not as important for imaging steeply dipping features in a hard rock environment, as they are in petroleum applications. This is because the scale of the survey is much smaller, therefore the impact of scattering fields and velocity gradients are also smaller. However it was observed that random heterogeneous fields perturb the non-stationary phase contributors enough to ensure more effective cancellation of the non-physical events present in the CMP-sorted virtual source gathers. It is therefore expected that real data acquisition will result in a better virtual source image as the scattering nature of the earth medium will ensure less contamination from non-physical events.

It was also proven that the virtual source method is applicable for imaging features with complex geometries, and that the best final image is produced when a near-offset filter is applied to ensure only the true image rays are included in the data.

Finally, it was demonstrated that the surface source spacing is critical for ensuring effective destructive interference of the non-stationary phase contributions as it has the strongest control over the time difference range in the correlation gathers. The time difference range must be below the Ricker's Criterion to ensure optimal interference in the virtual source trace.

Chapter 6 Discussion

The purpose of this research is to investigate the virtual source method as a technique for imaging shallow, steeply dipping features. An example of such a scenario, are feeder dykes to the main ore body at Voisey's Bay mine (Figure 2). Imaging these feeder dykes, especially those associated with the mineralization, is important as understanding their orientation and location can aid the drilling program associated with underground deposit evaluations and development of the mine plan.

Due to the absence of turning waves in shallow hard rock environments, a straight ray tracing analysis is appropriate to understand how the virtual source method works, despite the inherent simplifications associated with it. The use of a ray tracing analysis enables both an in-depth understanding of the virtual source method and allows us to assess the impact of the acquisition parameters on the collected virtual source data. The work presented in Chapter 3 utilized the ray tracing analysis to demonstrate that the virtual source method is valid despite violating the requirement that buried receivers be surrounded completely by surface sources. The caveat to this observation however, is that the source density must be such that the incorrectly located events are sampled sufficiently, and the source aperture be broad enough to capture all the required image rays. The ray tracing analysis was also used in this Chapter to demonstrate that source aperture, receiver spacing and reflector location have a significant impact on the image ray fold and offset of the virtual source data. This conclusion is most important as it indicates that significant care must be taken in understanding what the required image ray geometry is and what image rays are actually captured by the walk-away VSP survey to ensure satisfactory virtual source data are acquired.

By understanding the impacts of acquisition geometry on the virtual source data, it is possible to analyze the virtual source data with greater insight in order to generate an optimal virtual source image. This was demonstrated in Chapter 4 by the generation of 2D synthetic walk-away VSP seismic data which was then converted into virtual source data via a cross correlation and summation process. Analysis of the pre-stack CMP-sorted virtual source gathers allowed for the identification of several features caused by the cross correlation process. These include a fundamental change in the character of the seismic events and a time shift in the data. The analysis of the pre-stack CMP gathers also highlighted features associated with the finite source aperture, such as the non-hyperbolic moveout of the uphole offsets, incorrect positioning and decrease in amplitude of the reflection events at near offsets and the presence of several events with no apparent physical meaning. Understanding these features allowed for an optimal final virtual source image to be generated.

Ultimately however, it is important to address the practical implementation issues associated with application of the method. Chapter 5 demonstrated several of these issues, including the impact of heterogeneous velocity and density fields, the ability of the virtual source method to image vertical features with complex geometries, and the importance of surface source spacing on ensuring effective destructive interference of the non-stationary phase contributions. The work in this Chapter demonstrated that heterogeneous velocity and density fields are not as important for imaging steeply dipping features in a hard rock environment, as they are in petroleum applications. This is because the scale of the survey is much smaller, therefore the impact of scattering fields and velocity gradients are also smaller. However it was observed that random heterogeneous fields perturb the non-stationary phase contributors enough to ensure more effective cancellation of the non-physical events present in the CMP-sorted virtual source gathers. It is therefore expected that real data acquisition will result in a better virtual source image as the scattering nature of the earth medium will ensure less contamination from non-physical events. It was also proven that the virtual source method is applicable for imaging features with complex geometries. Finally, it was demonstrated that the surface source spacing is critical for ensuring effective destructive interference of the non-stationary phase contributions.

This research has demonstrated that despite violating the requirement that buried receivers be surrounded completely by a continuous distribution of surface sources, the virtual source method is a valid technique for imaging shallow, steeply dipping features. The ray tracing analysis undertaken highlighted two important aspects of the methodology that cannot be violated, that being the sufficient capture and sampling of the image rays. In practice this is achieved via the careful selection of surface source aperture and spacing. By utilizing the ray tracing method to understand the limitations of realistic acquisition scenarios, optimal virtual source images of steeply-dipping features can be generated. Additionally, the ray tracing method is a versatile tool that applied geophysicists can readily use to understand their specific imaging problem to apply the virtual source method in practice.

Chapter 7 References

Aki, K., and B. Chouet, 1975, Origin of Coda Waves: Source, Attenuation, and Scattering Effects: J. Geophys. Res., 80, 3322–3342.

Bakulin, A., and Calvert, R., 2004, Virtual Source: New method for imaging 4D below complex overburden: 74th Annual International Meeting, SEG Extended Abstracts, 2477-2480.

Bakulin, A., and Calvert, R., 2005, Virtual shear source: A new method for shear wave seismic surveys: 75th Annual International Meeting, SEG Extended Abstracts, 2633-2636.

Bakulin, A., and Calvert, R., 2006, The virtual source method: Theory and case study: Geophysics, 71, SI139-SI150.

Bakulin, A., and Calvert, R., 2008, Virtual Source Method: overview of history and development: 78th Annual International Meeting, SEG Extended Abstracts, 2726-2730.

Caddigan, R., 2009, Imaging steep dipping geologic targets by combining both vertical borehole seismic acquisition and the virtual source method: B.Sc. (Hons) thesis, Memorial University of Newfoundland.

Claerbout, J.F., 1968, Synthesis of a layered medium from its acoustic transmission response: Geophysics, 33, 264-269.

Draganov, D., Wapenaar, K., and Thorbecke, J., 2003, Synthesis of the reflection response from the transmission response in the presence of white noise sources: 65th Annual International Conference and Exhibition, EAGE Extended Abstracts, P218.

Duff, D., 2007, Physical Property Analysis, Numerical and Scale Modeling for Planning of Surface Seismic Surveys: Voisey's Bay, Labrador: M.S. thesis, Memorial University of Newfoundland.

Fink, M., 1992, Time Reversal of Ultrasonic Fields – Part 1: Basic Principles: IEEE Transactions on Ultrasonics, Ferroelectrics, and Frequency Control, 39, no. 5, pp.555-566.

Frankel, A., and Clayton, R.W., 1986, Finite Difference Simulations of Seismic Scattering: Implications for the Propagation of Short-Period Seismic Waves in the Crust and Models of Crustal Heterogeneity: Journal of Geophysical Research, 91, no. B6, pp.6465-6489.

Haskell, N.A., 1941, The Relation Between Depth, Lithology, and Seismic Wave Velocity in Tertiary Sandstones and Shales: Geophysics, 6, 318-326.

Henley, D.C., 2008, Raypath interferometry: Statics in difficult places: 78th Annual International Meeting, SEG Extended Abstracts, 1263-1267.

Hornby, B.E., and Yu. J., 2006, Single-well imaging of a salt-flank using walkaway VSP data: 76th Annual International Meeting, SEG Extended Abstracts, 3492-3496.

Horton, C.W., 1955, The structure of the noise background of a seismogram: Geophysics, 20, 565-584.

Kallweit, R.S., and Wood, L.C., 1982, The limits of resolution of zero-phase wavelets: Geophysics, 47, 1035-1046.

Korneev, V., and Bakulin, A., 2006, On the fundamentals of the virtual source method: Geophysics, 71, A13-A17.

Lu, R., Willis, M.E., Campman, X., Ajo-Franklin, J., and Toksoz, M.N., 2007, Redatumming through a salt canopy – Another salt-flank imaging strategy: 77th Annual International Meeting, SEG Extended Abstracts, 3054-3058.

Lu, R., Willis, M.E., Mateeva, A., Lopez, J., and Toksoz, M.N., 2009, Imaging a salt dome flank by directional redatuming of a field 3D VSP survey: 79th Annual International Meeting, SEG Extended Abstracts, 4085-4088.

Mehta, K., Snieder, R., Calvert, R., and Sheiman, J., 2008, Acquisition geometry requirements for generating virtual-source data: The Leading Edge, 27, 620-629.

Naldrett, A.J., and Li, C., 2007, The Voisey's Bay deposit, Labrador, Canada in W.D. Goodfellow, ed., Mineral Deposits of Canada: A Synthesis of Major Deposit-Types, District Metallogeny, the Evolution of Geological Provinces, and Exploration Methods: Geological Association of Canada, Mineral Deposits Division, Special Publication No. 5, 387-407.

Oristaglio, M.L., 1985, A guide to current uses of vertical seismic profiles: Geophysics, 50, 2473-2479.

Rickett, J., and Claerbout, J., 1999, Acoustic daylight imaging via spectral factorization: helioseismology and reservoir monitoring: 69th Annual International Meeting, SEG Extended Abstracts, 1675-1678.

Schuster, G.T., 2001, Theory of Daylight/Interferometric Imaging: Tutorial: 63rd Annual International Conference and Exhibition, EAGE Extended Abstracts, A-32.

Schuster, G.T., 2009, Seismic Interferometry: Cambridge Press.

Schuster, G.T., and Zhou, M., 2006, A theoretical overview of model-based and correlation-based redatuming methods: Geophysics, 71, SI103-SI110.

Snieder, R., Wapenaar, K., and Larner, K., 2006, Spurious multiples in seismic interferometry of primaries: Geophysics, 71, SI111-SI124.

Vanconcelos, I., Gaiser, J., Calvert, A., and Calderon-Macias, C., 2008, Retrieval and suppression of surface waves using interferometry by correlation and by deconvolution: 78th Annual International Meeting, SEG Extended Abstracts, 2566-2570.

Wapenaar, K., 2004, Retrieving the elastodynamic Green's function of an arbitrary inhomogeneous medium by cross correlation: Physical Review Letters, 93, 254301.

Wapenaar, K., Draganov, D., and Robertsson, J., 2006, Introduction to the supplement of seismic Interferometry: Geophysics, 71, SI1-SI4.

Wapenaar, K., Draganov, D., Thorbecke, J., and Fokkema, J., 2002, Theory of acoustic daylight imaging revisited: 72nd Annual International Meeting, SEG Expanded Abstracts, 2269-2272.

Willis, M.E., Lu, R., Campman, X., Toksoz, M.N., Zhang, Y., and de Hoop, M.V., 2006, A novel application of time-reversed acoustics: Salt-dome flank imagine using walkaway VSP surveys: Geophysics, 71, A7-A11.

Xiao, X., Zhou, M., and Schuster, G.T., 2006, Salt-flank delineation by interferometric imaging of transmitted P- to S-waves: Geophysics, 71, SI197-SI207.

Xue, Y., Dong, S., and Schuster, G.T., 2009, Interferometric prediction and subtraction of surface waves with a nonlinear local filter: Geophysics, 74, SI1-SI8.

Yu, J., Byun, J., Seol, S.J., and Park, K.G., 2009, Effective monitoring for CO2 sequestration with virtual sources: 79th Annual International Meeting, SEG Extended Abstracts, 3855-3858.

Yu, J., and Hornby, B.E., 2007, Methods for interferometry imaging and application to VSP salt flank imaging: 77th Annual International Meeting, SEG Extended Abstracts, 3049-3053.

Zhou, R., Huang, L., Rutledge, J., Daley, T.M., and Majer, E.L., 2008, Using the coda-wave interferometry method and time-lapse VSP data to estimate velocity changes from geological carbon sequestration in a brine aquifer: 78^{th} Annual International Meeting, SEG Extended Abstracts, 3199-320

APPENDIX A

```
program RT_VSM

implicit none

!This is a very simple program that generates the "direct" and
!"reflected" waves to a geophone for a typical walk-away VSP set
!up.  The program then takes these geometrically calculated
!"direct" and "reflected" waves and uses a cross correlation and
!summation process to generate Virtual Source Data:
!
!
!___*___*___*___*___*___*___*<__xoff__>@<__xsalt__>|___Surface___
!                                     /|\          |
!                                      |           |
!                                      zg          |
!                                      |           |
!                                     \|/          |
!                                      g           |
!                                      |           |
!                                      |           | Salt Dome
!                                      |           | Reflectivity
!                                      g           | = 0.5
!                                      |           |
!                                      |           |
!                                      |           |
!                                      g           |
!                                      |           |
!                                      |           |
!                                      |           |
!                                      g           |
!                                      |           |
!                                      |           |
! * = Sources separated by n units
! g = geophone separated by m units
! Source 1 to Surface Borehole Location = xoff
! Surface Borehole Location to Salt Flank = xsalt
! Surface Borehole Location to First geophone = zg

integer, parameter :: n = 4
integer, parameter :: m = 1
real, parameter :: xoff = 1
real, parameter :: xsalt = 10
real, parameter :: zg = 20
integer, parameter :: numS = 25
integer, parameter :: numG = 11
real, parameter :: dt = 0.1 ! time interval
integer, parameter :: nt = 1500 ! total time interval

integer, parameter :: shot = 1 ! the virtual source gather to export
integer, parameter :: recv = 1 ! the crosscorrelated receiver
correlellogram to export for QC
integer, parameter :: time = 600 ! total time to export

real, dimension(numS, numG, nt) :: G, Gd, Gr
```

```
real, dimension(numG, numG, nt) :: T
real, dimension(numS, nt) :: cross
real, dimension(nt) :: Temp
real, dimension(nt) :: TempA, TempB

!Variables

real :: z1, z2
real :: dwave, rwave
integer :: dtime, rtime
integer :: i, j, k, o, l

open(20, file="VSP_Mod1S25S5R1.dat")
open(21, file="VS_Mod1S25S5R1.dat")
open(22, file="Corr_Mod1S25S5R1.dat")

call zeross(G, numS, numG, nt)
call zeross(T, numG, numG, nt)

!Generate the direct and reflection data

do i = 1, numS

      do j = 1, numG

            !Direct Wave

            dwave = sqrt((xoff+(i-1)*n)**2 + (zg+(j-1)*m)**2)
            dtime = dwave/dt

            !Reflected Wave

            rwave = sqrt((xoff+(i-1)*n+xsalt*2)**2 + ((j-1)*m+zg)**2)
            rtime = rwave/dt

            G(i,j,dtime) = 1
            G(i,j,dtime-1) = -0.5
            G(i,j,dtime+1) = -0.5

            Gd(i,j,dtime) = 1
            Gd(i,j,dtime-1) = -0.5
            Gd(i,j,dtime+1) = -0.5

            G(i,j,rtime) = 0.5
            G(i,j,rtime-1) = -0.25
            G(i,j,rtime+1) = -0.25

            Gr(i,j,rtime) = 0.5
            Gr(i,j,rtime-1) = -0.25
            Gr(i,j,rtime+1) = -0.25

      end do

end do
```

```
do j = 1, nt
      write(20,4) (G(1,k,j), k=1,numG)
end do


1 format(A6,i3)
2 format(A7,i3)
3 format(f10.1,f10.1)

! Now perform the virtual source redatuming.

!For each new common source gather (which is located at each receiver
location)


!For each trace in the common source gather (which is equal to the
number of receivers)

do k = 1, numG

      !For every other trace

      do l = 1, numG

      !For every shot

            do i = 1, numS

                  do o = 1, nt
                        TempA(o) = Gd(i,k,o) !Read in the receiver
information for the new virtual source
                        TempB(o) = Gr(i,l,o) !Read in the other receiver
information.
                  end do

                  call corr(TempA, TempB, nt, Temp)

                  if (k.eq.shot.and.l.eq.recv) then
                        do o = 1, nt
                        cross(i,o) = Temp(o)
                        end do
                  end if

                  do o = 1, nt
                        T(k,l,o) = T(k,l,o) + Temp(o)
                  end do
            end do
      end do
      print*, k, " of ", numG
end do

!end do
```

```
do j = 1, numG
      write(21,4) (T(shot,j,i), i=1,time)
end do

do j = 1, numS
      write(22,4) (cross(j,i), i=1,time)
end do

4 format(100000f5.1)

close(20)
close(21)
close(22)

contains
      subroutine zeross(A, l1, l2, l3)

      integer :: l1, l2, l3
      real :: A(l1,l2,l3)
      integer :: zssi, zssj, zssk

      do zssi = 1, l1
            do zssj = 1, l2
                  do zssk = 1, l3
                        A(zssi,zssj,zssk) = 0.0
                  end do
            end do
      end do

      end subroutine zeross

      subroutine zero(A, l1)

      integer :: l1
      real :: A(l1)
      integer :: zi

      do zi = 1, l1

            A(zi) = 0.0

      end do

      end subroutine zero


      subroutine corr(A, B, ln, xc)

      ! This computes the lags only

      integer :: ln
      real :: A(*), B(*), xc(*)
      integer :: ci, cj, ck
```

```
      call zero(xc, ln)

      do ci = 1, ln

            ck = 1

            do cj = ci, ln

                  xc(ci) = xc(ci) + A(ck)*B(cj)
                  ck = ck + 1

            end do

      end do

      end subroutine corr

end program RT_VSM
```

APPENDIX B

```
program CMP2surf

!This simple program reads in the total number of downhole
!receivers, receiver spacing, distance of borehole from the
!reflector and the depth to first receiver from a file and then
!computes the surface source locations required to satisfy each
!Virtual Source CMP and the offset value of the VS trace
!contributing to a particular downhole CMP location.

implicit none

!Definitions
!NumRx : Total number of receivers downhole
!RxInt : Interval between receivers
!CMPNum : CMP Number, starting at 1 at the top of the hole
!TotalCMP : Total number of CMP's
!TrueCMP : True location of the CMP from the surface
!RelCMP : CMP location relative to the first Rx
!RefDx : Distance of the vertical borehole from the vertical
!     reflector
!dz : Depth to the first Rx
!x : Distance to surface shot location
!offset : Offset distance from CMP to Rx/VS location.

! ShotInt
!  <-->
!--*--*--*--*---------------------------------|-------------|
!           <-----------------x-------------->|<---RefDx--->| ^
!                                             |             | |Dz
!                                             |             | |
!                                     ^-------@_____________|_V
!                                     |RxInt  |             |
!                                     V-------@ Rx          |
!                                             |             | Ref
!                                             @ Borehole    |
!                                             |             |
!                                             @             |
!                                             |             |
!
!
!Virtual Source View
!                         RelCMP
!                          |<-->|           |
!____________@_______@_____|____*___________|
!                     \        /            |
!                      \   |<-/--TrueCMP--->|  Surface
!                       \    /              |
!                        \  /               |
!_________________________\/________________|_
```

```
!Set Parameters

!integer, parameter :: NumRx=100
!real, parameter :: RxInt=2.5
!real, parameter :: RefDx=250.0
!real, parameter :: dz=50.0

integer :: NumRx
real :: RxInt
real :: RefDx
real :: dz

!Define other variables

integer :: CMPNum, i, j, k, TotalCMP, Count, Output, filecount
real :: TrueCMP, RelCMP, x, offset, FirstCMP
real, dimension(1000,600,5) :: CMP
integer, dimension(1000) :: num, CMPCount
character(len=20) :: filename
character(len=20) :: numval

open(unit=2,file="param.dat")
read(2,*) NumRx, RxInt, RefDx, dz
print*, NumRx, RxInt, RefDx, dz

!Calculate initial variables

FirstCMP = RxInt/2
TotalCMP = ((NumRx-1)*2) - 1

filecount=1

!Set up CMP 3D matrix

do i = 1, TotalCMP
      CMPCount(i) = 0
end do

do i = 1, (NumRx-1)

   print*, "Virtual Source Number: ", i
   print*,

      do j = (i+1), NumRx
            Offset = ((j-i)*RxInt)/2
            RelCMP = Offset + (i-1)*RxInt
            TrueCMP = RelCMP + dZ
            x = (TrueCMP*(RefDx/Offset)) - RefDx

            CMPNum = RelCMP/FirstCMP

            Count = CMPCount(CMPNum)
            Count = Count + 1
```

```
            CMPCount(CMPNum) = Count
            CMP(CMPNum, Count, 1) = Count
             CMP(CMPNum, Count, 2) = TrueCMP
             CMP(CMPNum, Count, 3) = RelCMP
             CMP(CMPNum, Count, 4) = Offset
             CMP(CMPNum, Count, 5) = x


      end do
end do

CMP(Output,1,2)
CMP(Output,1,3)

open(unit=3, file="CMP2surf_x_Dec.dat")
do i = 1, TotalCMP, 10
   do j = 1, CMPCount(i)
      write(3,*) i, CMP(i,j,5)
   end do
end do

open(unit=3, file="CMP2surf_offset_Dec.dat")
do i = 1, TotalCMP, 10
   do j = 1, CMPCount(i)
      write(3,*) i, CMP(i,j,4)
   end do
end do

end program CMP2surf
```

```
program surf2CMP

!This simple program reads in the total number of downhole
!receivers, receiver spacing, distance of borehole from the
!reflector, depth to first receiver, total shot number and shot
!interval from a file and then determines what affect the surface
!source distribution has on the downhole Virtual Source CMP
!offsets.

implicit none

!Definitions
!NumShot : Total number of shots on the surface
!ShotInt : Interval between shots - Note that the first shot location is
SxInt from the borehole
!NumRx : Total number of receivers downhole
!RxInt : Interval between receivers
!CMPNum : CMP Number, starting at 1 at the top of the hole
!TotalCMP : Total number of CMP's
!TrueCMP : True location of the CMP from the surface
!RelCMP : CMP location relative to the first Rx
!RefDx : Distance of the vertical borehole from the vertical
!      reflector
!dz : Depth to the first Rx
!x : Distance to surface shot location
!offset : Offset distance from CMP to Rx/VS location.
!TotalX : Total shot range from the borehole
!AcptEr : Acceptable error for determing the surface source
!      number
!ShotNum : Shot number
!ShotAct : Fractional shot number
!Frac : Difference between ShotAct and ShotNum

! ShotInt
!  <-->
!--*--*--*--*---------------------------------|-------------|
!           <-----------------x-------------->|<---RefDx--->| ^
!                                             |             | |Dz
!                                             |             | |
!                                    ^-------@_____________|_V
!                                    |RxInt  |             |
!                                    V-------@ Rx          |
!                                             |             | Ref
!                                             @ Borehole    |
!                                             |             |
!                                             @             |
!                                             |             |
!
!
!
!
!
!
!
```

```
!Virtual Source View
!                         RelCMP
!                          |<-->|           |
!____________@_______@_____|____*___________|
!                     \        /            |
!                      \   |<-/--TrueCMP--->|  Surface
!                       \    /              |
!                        \  /               |
!_________________________\/________________|_

!Set Parameters

!integer, parameter :: NumRx=100
!real, parameter :: RxInt=2.5
!real, parameter :: RefDx=250.0
!real, parameter :: dz=50.0

integer :: NumRx, NumShot
real :: RxInt, ShotInt
real :: RefDx
real :: dz

!Define other variables

integer :: CMPNum, i, j, k, TotalCMP, Count, Output, filecount, ShotNum
integer :: Dn, Up, ShotDn, ShotUp
real :: TrueCMP, RelCMP, x, offset, FirstCMP, TotalX, ShotAct, AcptEr,
Frac
real :: DistDn, DistUp
real, dimension(1000,600,5) :: CMP
integer, dimension(1000) :: num, CMPCount
character(len=20) :: filename
character(len=20) :: numval

open(unit=2,file="param_surf2CMP.dat")
read(2,*) NumShot, ShotInt, NumRx, RxInt, RefDx, dz
print*, NumShot, ShotInt, NumRx, RxInt, RefDx, dz

!Calculate initial variables

FirstCMP = RxInt/2
TotalCMP = ((NumRx-1)*2) - 1
TotalX = ShotInt*NumShot
print*, "X Total = ", TotalX
print*, "What is the average wavelength expected?"
read*, AcptEr
AcptEr = AcptEr/2

filecount=1

!Set up CMP 3D matrix

do i = 1, TotalCMP
```

```
      CMPCount(i) = 0
end do

do i = 1, (NumRx-1)

   print*, "Virtual Source Number: ", i
   print*,

   do j = (i+1), NumRx
      Offset = ((j-i)*RxInt)/2
      RelCMP = Offset + (i-1)*RxInt
      TrueCMP = RelCMP + dZ
      x = (TrueCMP*(RefDx/Offset)) - RefDx
      CMPNum = RelCMP/FirstCMP

      if (x.lt.TotalX) then

         ShotAct = x/ShotInt
         ShotNum = nint(ShotAct)
         Frac = abs(ShotNum - ShotAct)

         Dn = floor(x/ShotInt)
         ShotDn = Dn*ShotInt
         DistDn = x - ShotDn

         Up = ceiling(x/ShotInt)
         ShotUp = Up*ShotInt
         DistUp = ShotUp - x

         if (DistUp.le.AcptEr .OR. DistDn.le.AcptEr) then
            print*, "ACCEPTED"

            Count = CMPCount(CMPNum)
            Count = Count + 1

            CMPCount(CMPNum) = Count
            CMP(CMPNum, Count, 1) = Count
            CMP(CMPNum, Count, 2) = TrueCMP
            CMP(CMPNum, Count, 3) = Offset
            CMP(CMPNum, Count, 4) = x
            CMP(CMPNum, Count, 5) = ShotNum

         end if
      end if
   end do
end do

CMP(Output,1,2)
CMP(Output,1,3)

open(unit=3, file="surf2CMP_40_60Int_offset_ALL.dat")
!do i = 1, TotalCMP, 10
do i = 1, TotalCMP
   do j = 1, CMPCount(i)
```

```
      write(3,*) i, CMP(i,j,3)
   end do
end do

end program surf2CMP
```

APPENDIX C

Homogeneous velocity models (and those with a simple vertical velocity gradient) are generated using the seismic un*x program unif2. The program requires a velocity model of the form:

VelMod1.txt

```
   0        0
5000        0
   1   -99999
   0     2396
3500     2396
3500        0
3750        0
3750     2396
   1   -99999
   0     2396
5000     2396
   1   -99999
   0     2400
5000     2400
   1   -99999
```

The format of the model is such that the line 1 -99999 indicates a new geometric layer.

VelModCreate is the shell code required to run the seismic un*x commands and create the velocity models.

VelModCreate

```
#! /bin/sh

# parameters for Virtual Source Modelling - Velocity Model 1&2&3
ninf=3 nx=1250 nz=600
dx=4 dz=4

# parameters for Forward Ground Truthing Modeling
#ninf=3 nx=850 nz=500
#dx=4 dz=4

# Create velocity model for Virtual Source Modelling - Velocity Model 1
```

```
#unif2 < VelMod1.txt ninf=$ninf nx=$nx nz=$nz dx=$dx dz=$dz
v00=6300,4500,6300 > VelMod1.bin

# Create velocity model for Forward Ground Truthing Modeling
#unif2 < VelMod1_FM.txt ninf=$ninf nx=$nx nz=$nz dx=$dx dz=$dz
v00=6300,4500,6300 >                VelMod1_FM.bin

# Create velocity model for Virtual Source Modelling - Velocity Model 2
#unif2 < VelMod1.txt ninf=$ninf nx=$nx nz=$nz dx=$dx dz=$dz \
#v00=6100,4500,6500 dvdz=0.17,0,0 > VelMod2.bin

# Create velocity model for Virtual Source Modelling - Velocity Model 3
unif2 < VelMod1.txt ninf=$ninf nx=$nx nz=$nz dx=$dx dz=$dz \
v00=6100,4500,6500 dvdz=0.464,0,0 > VelMod3.bin

#create density model for Virtual Source Modelling - Velocity Model 1
#unif2 < VelMod1.txt ninf=$ninf nx=$nx nz=$nz dx=$dx dz=$dz
v00=2.7,4.5,2.7 > DenMod1.bin

#create density model for Forward Ground Truthing Modeling
#unif2 < VelMod1_FM.txt ninf=$ninf nx=$nx nz=$nz dx=$dx dz=$dz
v00=2.7,4.5,2.7 >                DenMod1_FM.bin

#create density model for Virtual Source Modelling - Velocity Model 2
#unif2 < VelMod1.txt ninf=$ninf nx=$nx nz=$nz dx=$dx dz=$dz
v00=2.7,4.5,2.7 > DenMod2.bin

#create density model for Virtual Source Modelling - Velocity Model 3
unif2 < VelMod1.txt ninf=$ninf nx=$nx nz=$nz dx=$dx dz=$dz
v00=2.7,4.5,2.7 > DenMod3.bin

#ximage < VelMod1.bin n1=$nz d1=$dx d2=$dz &
#ximage < DenMod1.bin n1=$nz d1=$dx d2=$dz &
#ximage < VelMod1_FM.bin n1=$nz d1=$dx d2=$dz &
#ximage < DenMod1_FM.bin n1=$nz d1=$dx d2=$dz &
#ximage < VelMod2.bin n1=$nz d1=$dx d2=$dz &
#ximage < DenMod2.bin n1=$nz d1=$dx d2=$dz &
ximage < VelMod3.bin n1=$nz d1=$dx d2=$dz &
ximage < DenMod3.bin n1=$nz d1=$dx d2=$dz &

exit 0
```

Heterogeneous / random velocity models using a Gaussian or Two Phase distribution of velocity values are generated using more sophisticated code. These codes were supplied by Dr. C. Hurich and were not written by this author. The selfsim fortran code generates a random media provided input average velocity, a % rms variation, 2D correlation lengths and autocorrelation function order.

selfsim

```
c
c     A simple program to calculate a 2D random medium with a
c     von Karman autocorrelation function.  Different random media can
c     be generated by changing the autocorrelation function in the
c     fortran function frac.  See Frankel and Clayton for formulae for
c     different autocorrelation functions.
c
c     Ref:
c     Arthur Frankel and Robert Clayton, 1986,
c     "Finite Difference Simulations of Seismic Scattering:
c       Implications for the propagation of short-period Seismic waves
c       in the crust and models of crustal heterogeneity",
c     JGR, 91: 6465-6489
c
c     Written by Ted Charrette
c                MIT Earth Resources Lab
c                42 Carleton Street
c                Cambridge, MA 02142
c
c                e-mail: charrett@duchess.mit.edu
c                phone:  (617)-253-7872
c
c     WARNING: THIS PROGRAM WAS HACKED TOGETHER VERY QUICKLY
c     AND MAY STILL CONTAIN ERRORS <eecIII>
c
c
c     Modified by Bent O. Ruud    (June 1991)
c                 Oslo University
c                 Dept of Geology
c                 P.O. Box 1047, Blindern
c                 N-0316 Oslo 3, Norway
c
c                 e-mail: bentr@granitt.uio.no
c                   or  : bent@trane.norsar.no
c
c     Input parameters (read from input file 'ranmod.inp'):
c
c           dx, dy : sampling interval in x and y direction
c           nx, ny : number of grid points in x and y direction
c           percnt : percentage rms variation
c           ax, ay : correlation lengths in x and y direction
c           nu     : order of von Karman function,
c                    self-similar medium for nu=0.,
c                    exponential medium for nu=0.5,
c                    fractal dimension is (3-nu)
```

```
c          aver   : average velocity of the medium
c          iseed  : seed for random number generator
c          fname  : name of output file
c          form   : format used in output file
c          heading: a character string written in first record
c                   of the output file
c
```

NOTE: Run the selfsim executable. DO NOT COMPILE selfsim.for. There is an error in this code and the program WILL NOT RUN. Use the already existing selfsim executable, and modify parameters in the ranmod.inp.

ranmod.inp

```
dx        dy       nx       ny
4         4        1250     600
%rms      ax       ay       order      ave.       iseed
3         150      150      0.3        5900       35317

filename.dat                 (f8.1)

0.3 order VonKarmon,ax=0.15 km ay=0.15,rms=3%
```

In order to ensure compatibility with the homogeneous velocity models ensure that dx, dy, nx and ny are 4, 4, 1250 and 600 respectively.

Two velocity / density models are generated using the selfsim code. The first model used a 0.3 von Karman value to model a Gaussian distribution, whilst the second utilised a 0.15 von Karman value. The velocity and density files generated using the 0.15 value was then input into the fortran code twophase.for to transform the 3% randomly distributed media into a 3% bimodally distributed media.

Velocity Model – Gaussian

```
dx      dy      nx      ny
4       4     1250     600
%rms    ax      ay      order     ave.      iseed
3       150     150      0.3      5900      35317
```

Density Model – Gaussian

```
dx      dy      nx      ny
4       4     1250     600
%rms    ax      ay      order     ave.      iseed
3       150     150      0.3      2.7     35317
```

Velocity Model – Two Phase

```
dx      dy      nx      ny
4       4     1250     600
%rms    ax      ay      order     ave.      iseed
3       150     150      0.15     5900      35317
```

Velocity Model – Two Phase

```
dx      dy      nx      ny
4       4     1250     600
%rms    ax      ay      order     ave.      iseed
3       150     150      0.15      2.7      35317
```

twophase.for

```
c ---  Program to convert Gaussian velocity file to
c      a binary (wrt velocity) function
```

```
      character*25 infile,outfile
      integer*8 i
      integer*8 kount
      real*8 totvel

      print*,''
      print*,'Name of INPUT FILE :'
      read(*,*)infile
      print*,''
      print*,'Name of OUTPUT FILE :'
      read(*,*)outfile
      print*,''

      print*,'Assign Low velocity:  '
      read(*,*)velow
      print*,'Assign High velocity:  '
      read(*,*)velhi

      open(unit=2,file=infile)

      totvel=0.0
      kount=0
      vel=0.0

      do 10 i=1,50000000
         read(2,*,end=11)vel
         totvel=totvel+vel
         kount=kount+1
10    continue

11    continue

      avevel=totvel/kount
      print*,'totvel = ',totvel
      print*,'# of grids = ',kount
      print*,'Average velocity =  ',avevel

      close(2)

      open(unit=2,file=infile)
      open(unit=3,file=outfile)

      do 20 i=1,kount
         read(2,*)val

         if(val.ge.avevel) then
            write(3,*)velhi
         else
            write(3,*)velow
         endif
20    continue

      stop
```

```
end
```

The low and high velocity / density values (based on the 3% rms variation) required for the twophase.for program are:

Vlow = 2723 m/s; Vhigh = 6077 m/s; Dlow = 2.619 gcc; Dhigh = 2.781 gcc

Note that the parameters utilised for the modelling are based on the physical parameters measured from rocks at the Voisy's Bay mine.

These random velocity models are simply for the background medium and still require the vertical dyke velocities to be inserted. The fortran program blockfil.f90 performs this task.

blockfil.f90

```
program blockfil

implicit none

!This simple program to block fill in velocities based on vertical
coordinates

integer, parameter :: nx = 1250
integer, parameter :: nz = 600
integer, parameter :: blkx1 = 875
integer, parameter :: blkx2 = 938

integer :: column, row, numval, i, j
```

```
real, dimension(nx,nz) :: velorg

numval=nx*nz

!open the file to be modified and read in the velocities
i=0
j=0

open(unit=1,file="v5900tp.dat")
!open(unit=1,file="d2p7tp.dat")
do i = 1,numval
      column=int((i-1)/nz) + 1
      row = i - (column-1)*nz
      read(1,*)velorg(column,row)
!     print*, velorg(column,row)
end do
close(1)

print*, column, nx, row, nz

do i = 1, nx
      if (i.ge.blkx1.and.i.le.blkx2) then
            do j = 1, nz
                  velorg(i,j) = 4500.0
                  !velorg(i,j) = 4.5
            end do
      end if
end do

open(unit=22, file="VelModtp.dat")
!open(unit=22, file="DenModtp.dat")

do i = 1, nx
      do j = 1, nz
            write(22,4) (velorg(i,j))
!           print*, velorg(i,j)
      end do
end do
close(22)
4 format(f8.1)

end program blockfil
```

The previous models generated all utilized simple geometries that could be easily defined. For more complex geometries images can be created as an image and then converted into a velocity file. The following is the process to do this. Note that convertpcx was supplied by Dr. C. Hurich and was not written by this author.

convertpcx

```
#!/bin/bash
input=$1

( pcxtoppm < ${input} | \
  ppmtopgm             | \
  pnmflip -transpose   | \
  pnmtoplainpnm        | \
  sed -e '1,3d'        | \
  tr -s ' ' '\n'       ) 2> /dev/null

exit 0
```

NOTE: That the image must have the same number of pixels as grid points expected in the model.

```
chmod +x convertpcx
./convertpcx ComplexModel.pcx > ComplexModel.txt
a2b n=1 < ComplexModel.txt > ComplexModel.bin
ximage n1=600 legend=1 < ComplexModel.bin

./fillvel2
# of grids in Z direction (rows)
600
 # of grids in X direction (cols)
1250
 # of velocity fields: "
2
Name of INPUT FILE 1 :
4500.txt or 4.5.txt
Range of Values to be detected -- min,max
0,200
Name of INPUT FILE 2 :
6300.txt or 2.7.txt
Range of values to be detected -- min,max
201,255
 Name of MODEL FILE :
ComplexModel.txt
ComplexModel.txt.vel or ComplexModel.txt.den

a2b n1=1 < ComplexModel.txt.vel > ComplexModelVel.bin or
a2b n1=1 < ComplexModel.txt.den > ComplexModelDen.bin
```

```
ximage n1=600 legend=1 < ComplexModelVel.bin
ximage n1=600 legend=1 < ComplexModelDen.bin
```

Then in order for the velocity model to be used in the following synthetic modelling code, the ascii file must be converted into binary format.

```
a2b < filename.dat n2=600 > filename.bin
```

VSP_Shoot

```
#! /bin/sh
# Function: Shoot into fixed receiver array.
#         convert windowed su file to straight binary file

# Get windowing information

shotnum=1
shotinc=8
# Note that shotinc is in distance and must be a multiple of the
#horizontal grid spacing in the vel file.
shotx=3236
#velfile="VelModl.bin"
#denfile="DenModl.bin"
#shotfile="ShotModl.bin"
#velfile="VelMod2.bin"
#denfile="DenMod2.bin"
#shotfile="ShotMod2.bin"
#velfile="VelMod3.bin"
#denfile="DenMod3.bin"
#shotfile="ShotMod3.bin"
#velfile="VelModgaus.bin"
#denfile="DenModgaus.bin"
#shotfile="ShotModgaus.bin"
velfile="VelModtp.bin"
denfile="DenModtp.bin"
shotfile="ShotModtp.bin"
filename="Modtp"

count=0

rm movie_$filename.su
rm VSPData_$filename.sgy

#shots should be 180
echo -n "     Number of shots to take: "
read total

while [ $count -lt $total ]; do
```

```
        # Finite difference modeling
        echo shotx = "$shotx"
        echo count = "$count"
        echo

        echo Start FD modeling
        echo

        sufdmod2 < $velfile  > /dev/null \
        dx=4 dz=4 \
        nx=1250  nz=600 \
        fmax=80 \
        xs=$shotx \
        zs=4 \
        vsx=3252 \
        tmax=0.6  \
        abs=1,1,1,1 \
        dfile=$denfile \
        vsfile=$shotnum.su \
        verbose=1
        echo
        echo FD modeling complete
        echo

        suwind < $shotnum.su > $shotnum.window key=tracl min=1 max=300

        # Resample the seismogram
        suresamp < $shotnum.window nt=600 dt=0.001 | sushw key=tracr a=1
b=1 > $shotnum.resamp
        cat $shotnum.resamp >> movie_$filename.su
        echo resample complete
        echo
        rm $shotnum.su
        rm $shotnum.resamp
        rm $shotnum.window

        shotnum=`echo $shotnum+1 | bc`

        count=`echo $count+1 | bc`
        shotx=`echo $shotx-$shotinc | bc`

        date
        echo

done

# Convert to segy
segyhdrs < movie_$filename.su
segywrite endian=0 tape=VSPData_$filename.sgy < movie_$filename.su

echo finished
date
```

```
suxmovie < movie_$filename.su n2=300 title="frame=%g" loop=1 clip=0.05

exit 0
```

APPENDIX D

Read the VSPData.sgy into Promax to perform simple bandpass filtering and to generate the files required for the cross correlation.

IMPORT DATA

SEG-Y Input	
Type of SEG-Y	Standard fixed trace length
Type of storage to use	Disk
Select disk file type	Disk Image
Enter DISK file path name	/net/tapebox/public_2/users/ebrand/data/ FDMod/ Mod1/VSPData.sgy
Browse for DISK file path name	Browse
Update LIN database at end of input?	Yes
Override input data's sample interval?	No
Samples per data trace (override binary header)	0
Store reel header in processing history?	Yes
Input AUXILIARY traces?	Yes
Get CHANNEL NUMBER from trace headers?	No
Input trace FORMAT	Get from header
Apply trace weighting factors (2**-N)?	No
Display ensemble information?	Yes
Maximum TIME to input	0.
Is this STACKED data?	No
MAX traces per ensemble	300
Primary SORT header word (domain of data)	SHOT
Input PRIMARY selection choice?	Input ALL
Input SECONDARY selection choice?	None
Input Global XY reference coordinates?	No
Use the coordinate scalar?	No
Scan the range of all header words?	Yes
Use SEG-Y Rev 1 header mapping?	Autodetect
Remap SEG-Y header values?	No
Trace Header Math	
Select Mode	Sequence renumber mode
Renumber ensembles or traces?	TRACES
SELECT trace header word	Recording channel number
Starting value	1
Increment value	1
Extract Database Files	
Is this a 3D survey?	No
Data type	Land
Source index method	FFID
Receiver index method	STATIONS
Mode of operation	OVERWRITE
Pre-geometry extraction?	Yes
Extract CDP binning?	No
Calculate trace midpoint coordinates?	Yes
Extract OFB binning?	No

Trace Header Math

Select Mode	Sequence renumber mode
Renumber ensembles or traces?	ENSEMBLES
SELECT trace header word	Field file ID number
Starting value	1
Increment value	1

Disk Data Output

Ouput Dataset Filename	VSP_Mod1
New, or Existing, File?	New
Record length to output	0.
Trace sample format	32 bit
Skip primary disk storage	No

GEOM

Disk Data Input

Read data from other lines/surveys?	No
Select dataset	VSP_Mod1
Propagate input file history	Yes
Trace read option	Get ALL
Read the data multiple times?	No
Process trace headers only?	No
Override input data's sample interval?	No

*VSP Geometry Spreadsheet**
{Execute This Flow to get the VSP Geometry Assignment Tool Bar}

Sources

{Ensure that the number Mark Block is equal to the total number of shots (in this case 180) and set Source and Station to increment from 1 to 180. Set X to first source location in the model (3236) and set the increments to -8 (the source spacing). Y (set all to 0), Elev (set all to 0), Pat Depth (set all to 0), FFID (increment from 1 to 180), Tool Az (set all to 0), Uphole (set all to 0.6), Hole Depth (set all to -4.0), Pattern (set all to 1), Num Chan (set all to 300), Static (set all to 0).}

Patterns

Mark Block	Pattern	Min Chan	Max/Gap Chan	Chan Inc	Grp Int	Offset	Delta Az
1	1	1	300	1	4	0	0

{Ensure that NChans is set to 300 (find this parameter under the Edit drop down menu)}

Bin

<Assign geometry by patterns>
<Ok>

<Bin midpoints>
<Ok>

<Finalize Database>
<Ok>

{Provided that there are no errors}

<Cancel>

{Use TraceQC to ensure all the values are correct}

{Exit out of VSP Geometry Spreadsheet* and make the process inactive}

{Now activate...}

Inline Geom Header Load	
Primary header to match database	FFID
Secondary header to match database	None
Match by valid trace number?	No
Verbose diagnostics?	No

{This will then apply the geometry that we set up using the VSP Geometry Spreadsheet to the file, but this new file must be exported}

Disk Data Output	
Ouput Dataset Filename	VSP_Mod1geom
New, or Existing, File?	New
Record length to output	0.
Trace sample format	32 bit
Skip primary disk storage	No

DISPLAY {Use this to pick mutes for scattering analysis}

Disk Data Input	
Read data from other lines/surveys?	No
Select dataset	VSP_Mod1geom
Propagate input file history	Yes
Trace read option	Get ALL
Read the data multiple times?	No
Process trace headers only?	No
Override input data's sample interval?	No

Trace Display	
Select display DEVICE	This Screen
Specify display START time	0.
Specify display END time	0.
Maximum number of TRACES/screen	300
Traces to overlap between screens	0
Number of ENSEMBLES(line segments)/screen	4
Trace GAP between ensembles	1.
Do you want to use variable trace spacing?	No
Output Mode	When Done
Trace display MODE	Grayscale
Display color bar?	No
Header Plot Parameter	No trace header selected
Automatically SAVE screens?	Yes

Maximum number of screen images to save	10
Save screens in Color?	Yes
Where to save screen images	Xserver
Number of screens to collect	1
DIRECTION of trace plotting	Left to right
POLARITY of trace display	Normal
Primary trace LABELING header entry	Field file ID number
Secondary trace LABELING header entry	Recording channel number
MODE of Secondary trace annotation	Incremental
INCREMENT for Secondary trace annotation	5
Trace scaling mode	Conventional
Trace excursion at which to CLIP	2
SCALAR for sample value multiplication	1
Trace scaling option	Individual
Trace Orientation	Vertical

SPECANAL

Disk Data Input

Read data from other lines/surveys?	No
Select dataset	VSP_Mod1geom (for inital analysis)
Propagate input file history	Yes
Trace read option	Get ALL
Read the data multiple times?	No
Process trace headers only?	No
Override input data's sample interval?	No

{Analyse the VSP data to determine what sort of bandpass filter will be necessary to apply prior to the crosscorrelation}

Interactive Spectral Analysis

Data selection method	Simple
Display data by traces or ensembles?	Traces
Number of traces per analysis location	300
Number of traces between analysis locations	0
Primary header for sorting and trace label	Recording channel number
Secondary header for sorting and trace label	No trace header entry selected
Display the average power spectrum?	Yes
Type of scaling for power spectrum	Percent Power
Type of mapping for power spectrum	Linear
Reference power	-1
Display the average power spectrum	Yes
Time, sample, linear or no phase shift?	None
Unwrap the phase spectrum?	No
Display the selected trace data?	Yes
Display the FX power spectrum?	Yes
Display the pre-FFT time window?	No
Pre-FFT time window taper type	Hanning
Percent flat for the pre-FFT time window	80
Set frequency display ranges automatically?	Yes
Set power display ranges automatically?	Yes
Set phase display ranges automatically?	Yes

Bandpass Filter

TYPE of filter	Single Filter
Type of filter specification	Ormsby bandpass
PHASE of filter	Zero
Domain for filter application	Frequency
Percent zero padding for FFT's	25
Apply a notch filter?	No
Ormsby filter frequency values	0-15-385-400
Re-apply trace mute after filter?	No

{F-K analysis for visualisation of the effects of scattering on the energy of the direct wave}

F-K Analysis <= FK

Panel width in traces domain)	300 (if in shot domain) 180 (if in receiver
Starting time for analysis	0
Ending time for analysis	0
Distance between input traces domain)	4 (if in shot domain) 8 (if in receiver
Starting display configuration	TX-FK
Position of zero wavenumber in display	CENTER
Position of zero frequency in display	BOTTOM
Plot FK, TK, TX panels in DB or Linear	DBSCALE
Initial TX gain setting (percentile)	98
Initial FK maximum gain setting (db)	0
Initial FK minimum gain setting (db)	0
Percent flat for trace ramping	100
Percent flat for time ramping	100
Select mute polygon table	FK
Mode of F-K filter operation	REJECT
Percent flat for F-K filter windowing	90
Time length for F-K filter (ms)	500
Spatial extent of F-K filter (traces)	50

Disk Data Output

Ouput Dataset Filename	VSP_Mod1BP
New, or Existing, File?	New
Record length to output	0.
Trace sample format	32 bit
Skip primary disk storage	No

EXPORTDATA

Disk Data Input

Read data from other lines/surveys?	No
Select dataset	VSP_Mod1BP
Propagate input file history	Yes
Trace read option	Get ALL
Read the data multiple times?	No
Process trace headers only?	No
Override input data's sample interval?	No

SEG-Y Output

Type of SEG-Y	Standard
Type of storage to use	Disk Image
Enter DISK file path name	/net/tapebox/public_2/users/ebrand/data/ FDMod/Mod1/VSPData.sgy
Polarity of output data	NORMAL
EBCDIC Reel Header Generation Method	User type in
Edit (copy) SEG-Y reel header	C 1 CLIENT
Display dataset information option	None
Job ID # for binary header	1
Line # for binary header	1
Desired trace format	IBM Real
Maximum time to output	0.
Remap SEGY header values?	No

Converting SGY Data into SU format

```
segyread tape=VSP_Data.sgy over=1 endian=0 ns=600 conv=0 | segyclean >
VSP_Data.su
```

Cross Correlation Process to Generate Virtual Source Data

XCorr

```
#! /bin/sh
# The purpose of this program is to xcorrelate shot records with a
specified chan
# within each of the shots to simulate a new virtual source location.

firstVS=1
lastVS=300
#VStotal=11
VStotal=300
RXtotal=300
Stotal=180
#dwave="VSP_DATAMod1_BP.su"
#rwave="VSP_DATAMod1_BP.su"
#filename="Mod1"
#dwave2="VSP_DataBP2.su"
#rwave2="VSP_DataBP2.su"
#dwave3="VSP_DataBP3.su"
#rwave3="VSP_DataBP3.su"
dwave="VSP_DATAModtp_BP.su"
rwave="VSP_DATAModtp_BP.su"
filename="Modtp"

VScount=1
RXcount=1

rm DW_VS.su
```

```
rm RW_RX.su
rm CorrGath.su
rm VSTrace.su
rm VSGath.su
rm VS_Data$filename.su
rm VS_DataCrop$filename.su

echo START OF CROSS CORRELATION

# For each trace

while [ $VScount -le $VStotal ]; do
    echo processing VS number "$VScount"
    suwind < $dwave key=tracl j=$lastVS s=$VScount | sushw key=tracl a=1
b=1 > DW_VS.su
# Cross correlate against every other trace and sum over all shots.
    while [ $RXcount -le $RXtotal ]; do
         echo processing VS number "$VScount" and RX number "$RXcount"
       suwind < $rwave key=tracl j=$lastVS s=$RXcount | sushw key=tracl
a=1 b=1 > RW_RX.su
       suxcor < RW_RX.su > CorrGath.su panel=1 sufile=DW_VS.su
       sushw < CorrGath.su key=cdp a=$VScount | sustack key=cdp
normpow=0 | sushw key=tracl              a=$RXcount > VSTrace.su
       cat VSTrace.su >> VSGath.su
       RXcount=`echo $RXcount+1 | bc`
    done

    cat VSGath.su >> VS_Data$filename.su
    rm VSGath.su
    RXcount=1
    VScount=`echo $VScount+1 | bc`

done

suwind < VS_Data$filename.su itmin=600 itmax=1200 >
VS_DataCrop$filename.su

echo END OF CROSS CORRELATION

# Convert to segy
segyhdrs < VS_Data$filename.su
segywrite endian=0 tape=VS_Data$filename.sgy < VS_Data$filename.su

# Convert to segy
segyhdrs < VS_DataCrop$filename.su
segywrite endian=0 tape=VS_DataCrop$filename.sgy <
VS_DataCrop$filename.su

exit 0
```

Import data into Promax for analysis, filtering, stacking and migration.

IMPORTDATA

SEG-Y Input	
Type of SEG-Y	Standard fixed trace length
Type of storage to use	Disk
Select disk file type	Disk Image
Enter DISK file path name	/net/tapebox/public_2/users/ebrand/data /FDMod/Mod1/VS_Data.sgy
Browse for DISK file path name	Browse
Update LIN database at end of input?	Yes
Override input data's sample interval?	No
Samples per data trace (override binary header)	0
Store reel header in processing history?	Yes
Input AUXILIARY traces?	Yes
Get CHANNEL NUMBER from trace headers?	Yes
Input trace FORMAT	Get from header
Apply trace weighting factors (2**-N)?	No
Display ensemble information?	Yes
Maximum TIME to input	0.
Is this STACKED data?	No
MAX traces per ensemble	300
Primary SORT header word (domain of data)	SHOT
Input PRIMARY selection choice?	Input ALL
Input SECONDARY selection choice?	None
Input Global XY reference coordinates?	No
Use the coordinate scalar?	No
Scan the range of all header words?	Yes
Use SEG-Y Rev 1 header mapping?	No
Remap SEG-Y header values?	No
Trace Header Math - #1	
Select mode	Sequence renumber mode
Renumber ensembles or traces?	TRACES
SELECT trace header word	External receiver location no. (SRF_SLOC)
Starting value	1
Increment value	1
Trace Header Math - #2	
Select mode	Sequence renumber mode
Renumber ensembles or traces?	ENSEMBLES
SELECT trace header word	Live source number (SOURCE)
Starting value	1
Increment value	1
Trace Header Math - #3	
Select mode	Sequence renumber mode
Renumber ensembles or traces?	ENSEMBLES
SELECT trace header word	Field file ID number (FFID)
Starting value	1
Increment value	1

Trace Header Math - #4

Select mode	Sequence renumber mode
Renumber ensembles or traces?	TRACES
SELECT trace header word	Recording channel number (CHAN)
Starting value	1
Increment value	1

Trace Header Math - #5

Select mode	Fixed equation mode
DEFINE trace header equation(s)	OFF=INT(-1*(SOURCE-CHAN)*4)

Disk Data Output

Ouput Dataset Filename	VS_Mod1
New, or Existing, File?	New
Record length to output	0.
Trace sample format	32 bit
Skip primary disk storage	No

GEOM

Disk Data Input

Read data from other lines/surveys?	No
Select dataset	VS_Mod1
Propagate input file history	Yes
Trace read option	Get ALL
Read the data multiple times?	No
Process trace headers only?	No
Override input data's sample interval?	No

*2D Land Geometry Spreadsheet**
{Execute This Flow to get the Land Geometry Assignment Tool Bar}

Setup

<SELECT> Matching pattern numbers using first live chan and station

Station Intervals (Generally Required; Please see Doc.)	
Nominal Receiver Station Interval:	4.0
Nominal Source Station Interval:	4.0

Station Range (Required)	
First Live Station Number	1
Last Live Station Number	300

Base Source station coordinates upon a match between source and receiver station numbers?
<Yes>

Source Type
<Surface seismic source>

Units
<Meters>

Select <Ok>

Receivers

{Input correct station and X coordinates. In this case stations are from 1 to 300 and X coordinates are from 0 to 1196m with 4m increments}

Sources

{Input Station, X coordinates, FFID (as equal to station), Offset (set all to 0), Skid (set all to 0), Pattern (set all to 1), Num Chan (set all to 300), 1st Live Station (set all to 1), 1st Live Chn (set all to 1), Gap Chan Dlt (set all to 0), Gap Size Dlt (set all to 0)}

Patterns

Mark Block	Pattern	Min Chan	Max/Gap Chan	Chan Inc	Rcvr MinChan	Rcvr MaxChan	Rcvr Inc	Error
1	1	1	300	1	1	300	1	

{Ensure that NChans is set to 300 (find this parameter under the Edit drop down menu)}

Bin

<Assign midpoint by: Matching pattern numbers using first live chan and station>
<Ok>

<Binning>
<Ok>

<Finalize Database>
<Ok>

{Provided that there are no errors}

<Cancel>

{Use TraceQC to ensure all the values are correct}

{Exit out of 2D Land Geometry Spreadsheet* and make the process inactive}

{Now activate...}

Inline Geom Header Load

Primary header to match database	FFID
Secondary header to match database	None
Match by valid trace number?	No
Drop traces with NULL CDP headers?	No
Drop traces with NULL receiver headers?	No
Verbose diagnostics?	No

{This will then apply the geometry that we set up using the 2D Land Geometry Spreadsheet to the file, but this new file must be exported}

Disk Data Output	
Ouput Dataset Filename	VS_Mod1_geom
New, or Existing, File?	New
Record length to output	0.
Trace sample format	32 bit
Skip primary disk storage	No

NMO

Disk Data Input	
Read data from other lines/surveys?	No
Select dataset	VS_Mod1Geom
Propagate input file history	Yes
Trace read option	Sort
Interactive Data Access?	No
Select primary trace header entry	CDP bin number
Select secondary trace header entry	No trace header entry selected
Sort order list for dataset	*/
Presort in memory or on disk?	Memory
Read the data multiple times?	No
Process trace headers only?	No
Override input data's sample interval?	No

Normal Moveout Correction	
Direction for NMO application	Forward
Stretch mute percentage	30
Apply any remaining static during NMO?	Yes
Disable check for previously applied NMO?	No
Apply partial NMO?	No
Long offset correction?	None
Get velocities from the database?	No
SPECIFY NMO velocity function(s)	1:0-6300 (velocity selected here depends on average for the model)

Disk Data Output	
Ouput Dataset Filename	VS_Mod1NMO
New, or Existing, File?	New
Record length to output	0.
Trace sample format	32 bit
Skip primary disk storage	No

STACK

Disk Data Input	
Read data from other lines/surveys?	No
Select dataset	VS_Mod1NMO
Propagate input file history	Yes
Trace read option	Sort
Interactive Data Access?	No
Select primary trace header entry	CDP bin number
Select secondary trace header entry	Signed source-receiver offset
Select tertiary trace header entry	No trace header entry selected
Sort order list for dataset	<Refer to trace filter options>
Presort in memory or on disk?	Memory

Read the data multiple times?	No
Process trace headers only?	No
Override input data's sample interval?	No

Bandpass Filter

TYPE of filter	Single Filter
Type of filter specification	Ormsby bandpass
PHASE of filter	Zero
Domain for filter application	Frequency
Percent zero padding for FFT's	25
Apply a notch filter?	No
Ormsby filter frequency values	0-10-80-90
Re-apply trace mute after filter?	No

CDP/Ensemble Stack

Sort order of input ensembles	CDP
MEHTOD for trace summing	Mean
Root power scalar for stack normalisation	0.5
Apply final datum statics after stack?	No
Has NMO been applied?	Yes

Disk Data Output

Ouput Dataset Filename	VS_Mod1_Stack
New, or Existing, File?	New
Record length to output	0.
Trace sample format	32 bit
Skip primary disk storage	No

MIGRATION

Disk Data Input

Read data from other lines/surveys?	No
Select dataset	VS_Mod1_Stack
Propagate input file history	Yes
Trace read option	Get All
Read the data multiple times?	No
Process trace headers only?	No
Override input data's sample interval?	No

Memory Stolt F-K Migration

Minimum CDP to migrate	2
Maximum CDP to migrate	600
CDP interval (ft or meters)	2
Maximum frequency to migrate (in Hz)	80
Get RMS velocities from database?	Yes
Select velocity file	6300 <Velocity file with constant velocity of 6300m/s>
Number of traces to smooth velocity field over	0
Percent velocity scale factor	100
Stolt stretch factor	0.6
Apply Stolt obliquity correction	Yes
Change maximum memory usage	No
Change default tapering?	No
Re-apply trace mutes?	Yes

Re-kill dead traces?	Yes
Trace Display	
Select display DEVICE	This Screen
Specify display START time	0.
Specify display END time	0.
Maximum number of TRACES/screen	600
Traces to overlap between screens	0
Number of ENSEMBLES(line segments)/screen	1
Do you want to use variable trace spacing?	No
Output Mode	When Done
Trace display MODE	Grayscale
Display color bar?	No
Header Plot Parameter	No trace header selected
Automatically SAVE screens?	Yes
Maximum number of screen images to save	10
Save screens in Color?	Yes
Where to save screen images	Xserver
Number of screens to collect	1
DIRECTION of trace plotting	Left to right
POLARITY of trace display	Normal
Primary trace LABELING header entry	CDP bin number
Secondary trace LABELING header entry	X coordinate of CDP
MODE of Secondary trace annotation	Incremental
INCREMENT for Secondary trace annotation	5
Trace scaling mode	Conventional
Trace excursion at which to CLIP	2
SCALAR for sample value multiplication	1
Trace scaling option	Individual
Trace Orientation	Vertical
Disk Data Output	
Ouput Dataset Filename	VS_Mod1_Mig
New, or Existing, File?	New
Record length to output	0.
Trace sample format	32 bit
Skip primary disk storage	No

APPENDIX E

```
program interfer

implicit none

!This is a simple program which generates a Ricker Wavelet of specified
!frequency and then generates the interference pattern for a series of
!stacked Ricker wavelets offset by a certain time increment.

!Set Parameters

!Define other variables

integer :: i, j, k, point, count, Det
real :: Freq, deltat
real :: dt, pi, Dtime
real, dimension(10000) :: R, IntR
character(len=20) :: filename

!Calculate initial variables

dt=0.0001
pi=3.14159265
Freq=40
deltat=0.008
Det=deltat/dt
print*, Det

do i = 1, 5000
   R(i) = 0
   IntR(i) = 0
end do

!Ricker Wavelet: R(t) = (1-2*pi**2*f**2*t**2)exp(-pi**2*f**2*t**2)

count=0

do i = -2500,2500
   count = count+1
   Dtime = i*dt
   R(count) = (1-2*pi*pi*Freq*Freq*Dtime*Dtime)*exp(-
pi*pi*Freq*Freq*Dtime*Dtime)
end do

do i=1,5000

   do j = i,5000,Det

      IntR(i) = IntR(i) + R(j)

   end do

end do

do i=5000,1,-1
```

```
      do j = i,1,-Det

         IntR(i) = IntR(i) + R(j)

      end do

   end do


   open(unit=3, file="Start_Trace.dat")
   do i = 1, 5000
      write(3,*) R(i)
   end do

   open(unit=3, file="Interference.dat")
   do i = 1, 5000
      write(3,*) IntR(i)
   end do

   open(unit=3, file="Both.dat")
   do i = 1, 5000-Det
      write(3,*) R(i+Det)
   end do
   do i = 1, Det
      write(3,*) 0
   end do
   do i = 1, 5000
      write(3,*) R(i)
   end do
   !do i = 1, 5000
   !   write(3,*) IntR(i)
   !end do


   end program interfere


   program deltat

   !This is a very simple program that generates the
   !reflected waves to a geophone for a typical walk-away VSP set
   !up.  The program then takes these geometrically calculated
   !reflected waves and computes the time difference between
   !the reflected waves for different shot records (which simulates the
   !cross correlation process.  The final output is a measurement of
   !time difference between the cross correlation event at adjacent
   !traces:

   implicit none

   !Definitions
   !NumShot : Total number of shots on the surface
```

```fortran
!ShotInt : Interval between shots - Note that the first shot location is
SxInt from the borehole
!NumRx : Total number of receivers downhole
!RxInt : Interval between receivers
!CMPNum : CMP Number, starting at 1 at the top of the hole
!TotalCMP : Total number of CMP's
!TrueCMP : True location of the CMP from the surface
!RelCMP : CMP location relative to the first Rx
!RefDx : Distance of the vertical borehole from the vertical reflector
!dz : Depth to the first Rx
!x : Distance to surface shot location
!offset : Offset distance from CMP to Rx/VS location.
!TotalX : Total shot range from the borehole
!AcptEr : Acceptable error for determing the surface source number
!ShotNum : Shot number
!ShotAct : Fractional shot number
!Frac : Difference between ShotAct and ShotNum


! ShotInt
!  <-->
!--*--*--*--*-------------------------------|------------
!           <-------x------->|<---RefDx---->|   ^
!                            |              |   | Dz
!                            |              |   |
!                 ^----------@______________|___V
!                 |RxInt     |              |
!                 V----------@ Rx           |
!                            |              | Reflector
!                            @  Borehole    |
!                            |              |
!                            @              |
!                            |              |
!

!Set Parameters

integer :: NumRx, NumShot
real :: RxInt, ShotInt, Vel
real :: RefDx
real :: dz

!Define other variables

integer :: i, j, ShotNum, tDCorr, tWCorr
integer :: true, IRNum, VSNum
real :: TotalX, Freq, Dtime, Wtime, DCorr, WCorr, DCorrPast, WCorrPast
real :: dt, pi, DA, DB, WA, WB
real, dimension(5000,5000) :: CorrGath
real, dimension(5000) :: VSTrace, DeltaTD, DeltaTW
character(len=20) :: filename
character(len=20) :: numval

open(unit=2,file="param_deltat.dat")
```

```
read(2,*) NumShot, ShotInt, NumRx, RxInt, RefDx, dz, Vel
print*, NumShot, ShotInt, NumRx, RxInt, RefDx, dz, Vel

!Calculate initial variables

TotalX = ShotInt*NumShot
dt=0.0001
pi=3.14159265
print*, "X Total = ", TotalX
print*, "What is the peak (of the) frequency (spectrum) expected?"
read*, Freq

!Find out which virtual source and which image receiver to use.

print*, "Which downhole receiver would you like to be the virtual
source?"
read*, VSNum
print*, "Which downhole receiver would you like to be the Image
Receiver?"
read*, IRNum

true=0

do while (true.eq.0)
      if (IRNum.gt.VSNum) then
            true=1
      else
            print*, "Image Receiver value is smaller than or equal to
the virtual source number, please choose a value greater than ", VSNum
            read*, IRNum
      end if
end do

!Compute "Crosscorrelation Gathers"

do i = 1, 5000
      VSTrace(i) = 0
      do j = 1, 5000
            CorrGath(i,j) = 0
      end do
end do

!Rciker Wavelet: R(t) = (1-2*pi**2*f**2*t**2)exp(-pi**2*f**2*t**2)

DCorrPast = 0
WCorrPast = 0

do i = 1, NumShot
print*, "Shot Number: ", i
!First compute the location of the direct and reflected events in the
crosscorrelation gather

      DA=sqrt((i*ShotInt)**2 + ((VSNum-1)*RxInt+dz)**2)/Vel
      DB=sqrt((i*ShotInt)**2 + ((IRNum-1)*RxInt+dz)**2)/Vel
```

```
      DCorr = DB-DA

!        print*, "DCorr = ", DCorr

!     WA=sqrt((i*ShotInt+2*RefDx)**2 + ((VSNum-1)*RxInt+dz)**2)/Vel
      WB=sqrt((i*ShotInt+2*RefDx)**2 + ((IRNum-1)*RxInt+dz)**2)/Vel

      WCorr = WB-DA

!        print*, "WCorr = ", WCorr

      tDCorr = DCorr/dt
      tWCorr = WCorr/dt

!        print*, "tDCorr = ", tDCorr
!        print*, "tWCorr = ", tWCorr

!     CorrGath(i,tDCorr) = CorrGath(i,tDCorr) + (1-
2*pi*pi*Freq*Freq*0)*exp(-pi*pi*Freq*Freq*0)
!     CorrGath(i,tWCorr) = CorrGath(i,tWCorr) + (1-
2*pi*pi*Freq*Freq*0)*exp(-pi*pi*Freq*Freq*0)

      do j = -1000,1000

            Dtime = j*dt
            Wtime = j*dt

                if (tDCorr+j.gt.0) then
                   CorrGath(i,tDCorr+j) = CorrGath(i,tDCorr+j) + (1-
2*pi*pi*Freq*Freq*Dtime*Dtime)*exp(-pi*pi*Freq*Freq*Dtime*Dtime)
                end if
                if (tWCorr+j.gt.0) then
                   CorrGath(i,tWCorr+j) = CorrGath(i,tWCorr+j) + (1-
2*pi*pi*Freq*Freq*Wtime*Wtime)*exp(-pi*pi*Freq*Freq*Wtime*Wtime)
                end if
      end do

!Now create the "Virtual Source Trace"

      do j = 1,5000
            VSTrace(j) = VSTrace(j) + CorrGath(i,j)
      end do

!Now create the delta T vector

      DeltaTD(i) = DCorrPast - DCorr
      DeltaTW(i) = WCorrPast - WCorr

      DCorrPast = DCorr
      WCorrPast = WCorr

end do
```

```
open(unit=3, file="CorrGath_80Hz_40m.dat")
do i = 1, NumShot
   do j = 1, 5000
      write(3,*) CorrGath(i,j)
   end do
end do

open(unit=3, file="VSTrace_80Hz_40m.dat")
do j = 1, 5000
      write(3,*) VSTrace(j)
end do

open(unit=3, file="deltat_DirectWave.dat")
do j = 1, NumShot
      write(3,*) j*ShotInt, DeltaTD(j)
end do

open(unit=3, file="deltat_ReflectedWave.dat")
do j = 1, NumShot
      write(3,*) j*ShotInt, DeltaTW(j)
end do

open(unit=3, file="deltat.dat")
do j = 2, NumShot
      write(3,*) j*ShotInt, DeltaTD(j), DeltaTW(j)
end do

end program deltat
```